ISSN 0280-5316
ISRN LUTFD2/TFRT--5906--SE

Trade-offs in Control of Switched Reluctance Motors

Olof Troeng

Lund University
Department of Automatic Control
October 2012

Lund University
Department of Automatic Control
Box 118
SE-221 00 Lund Sweden

Document name
MASTER THESIS

Date of issue
October 2012

Document Number
ISRN LUTFD2/TFRT--5906--SE

Author(s)
Olof Troeng

Supervisor
Scott Bartoff, Mitsubishi Electric Research Laboratories, Cambridge MA, USA
Anders Rantzer, Dept. of Automatic Control, Lund University, Sweden (examiner)

Sponsoring organization

Title and subtitle
Trade-offs in Control of Switched Reluctance Motors

Abstract
Soaring prices for rare earth metals have led to significantly increased production costs for permanent magnet motors. This has motivated research into alternative motor types, one of them, the switched reluctance motor (SRM), will be discussed in this thesis. The SRM has several positive and negative characteristics as well as highly nonlinear dynamics. It is not clear how trade-offs between these characteristics should be made in an optimal fashion when designing the motor hardware and control algorithm. An optimal control problem is formulated and the possibilities of using control to make trade-offs between torque ripple and efficiency is investigated. Based on the optimization results some possible improvements in SRM control are highlighted.

Keywords

Classification system and/ or index terms (if any)

Supplementary bibliographical information

ISSN and key title
0280-5316

ISBN

Language
English

Number of pages
1-69

Recipient's notes

Security classification

Trade-offs in Control of Switched Reluctance Motors

Olof Troeng

August 17, 2012

Abstract

Soaring prices for rare earth metals have led to significantly increased production costs for permanent magnet motors. This has motivated research into alternative motor types, one of them, the switched reluctance motor (SRM), will be discussed in this thesis. The SRM has several positive and negative characteristics as well as highly nonlinear dynamics. It is not clear how trade offs between these characteristics should be made in an optimal fashion when designing the motor hardware and control algorithm. An optimal control problem is formulated and the possibilities of using control to make trade-offs between torque ripple and efficiency is investigated. Based on the optimization results some possible improvements in SRM control are highlighted.

Acknowledgements

I would most of all like to express my gratitude to my advisor and host Dr. Scott Bortoff for letting me do my master's thesis as an intern at Mitsubishi Electric Research Laboratories (MERL), Cambridge, Massachusetts, USA.

Thank you Scott for introducing me to corporate research and for a truly amazing internship experience. Working with you has been very inspiring and has taught me a lot about a lot of things.

Thank you Professor Karl-Johan Åström for introducing me to Scott and for very insightful advice on career and academia.

Thank you Mats Alaküala at the Department of Industrial Electrical Engineering and Automation at Lund University for sharing your knowledge of motors and specifically switched reluctance motors.

Further thanks goes to all of the staff at MERL for being friendly and welcoming, in particular I would like to thank the researchers in the Mechatronics Group for many rewarding discussions related to my project and other things.

For making me interested in automatic control and teaching me most of what I know about the subject I would like to thank the Department of Automatic Control at Lund University.

My thanks also go to the friends that I have made during my time at Lund University and UC Santa Barbara and of course also my family, thank you all for being truly awesome.

Contents

Abstract . . . 3
Acknowledgements . . . 5
1. Introduction . . . 11
1.1 Background . . . 11
1.2 Problem formulation and objective . . . 12
1.3 Main Results . . . 13
1.4 Overview of the Thesis . . . 14
2. Background on Switched Reluctance Motors . . . 15
2.1 Introduction . . . 15
2.2 Basic SRM Concepts . . . 16
2.3 Generic Electrical Drive . . . 17
2.4 Energy Conversion Principle . . . 17
2.5 Converter Topology . . . 18
2.6 Control of SRMs . . . 19
3. Background on Optimal Control and Modeling Tools . . . 23
3.1 Optimal Control . . . 23
3.2 Collocation . . . 23
3.3 Modelica . . . 24
3.4 Optimica . . . 25
3.5 JModelica.org . . . 25
4. High Torque Density Switched Reluctance Motor Options 27
4.1 Low Loss Materials for Higher Torque Density . . . 27
4.2 Improved Slot-fill Factor . . . 27
4.3 High Torque-Density SRM Designs . . . 28
4.4 Selecting a Suitable Switched Reluctance Motor Topology . . . 29
4.5 The Segmented Switched Reluctance Motor . . . 30
5. Formulation of the optimal control problem . . . 33
5.1 Copper Loss Modeling . . . 33
5.2 Iron Loss Modeling . . . 33
5.3 Converter Modeling . . . 36
5.4 Electric Equations . . . 37
5.5 Mechanical Equations . . . 39
5.6 Thermal Modeling . . . 40
5.7 Constraints . . . 40
5.8 Objective Function . . . 41
5.9 Summary of the Optimal Control Problem . . . 41
6. Experiments and Results . . . 43
6.1 Experiment Procedure . . . 43
6.2 Test Case Type 1: Constant Velocity Operation . . . 43
6.3 Test Case 2: Point-to-point Movement . . . 56
7. Problem Structure . . . 59
8. Conclusion . . . 61
8.1 Pros and cons of using optimally designed phase trajectories . 61
9. Outlook and Future Work . . . 62
A. Bibliography . . . 63

List of Figures

1.1 The stator and rotor of an SRM used for a washing machine application [1]. 12
2.1 The needle of a compass and the rotor of the switched reluctance motor has the same tendency to align itself with the stream lines of the magnetic field that they are subjected to. . 15
2.2 The unaligned (left) and aligned rotor (right) positions for a 1-phase SRM [2]. 16
2.3 In images 1-3 it is seen how the rotor aligns itself with the energized phase to minimize the reluctance of the magnetic field. As the rotor has aligned itself with the active phase it is turned off and the next phase is turned on in order to keep the rotor in rotation as seen in figure 4-6. 16
2.4 A generic schematic of an electric motor drive system [2]. . . . 17
2.5 The magnetic energy and co-energy for a certain angle and a certain phase current correspond to the colored areas in the figure. 19
2.6 Typical flux linkage and torque curves for SRMs. 19
2.7 The asymmetric half bridge converter, the most common converter topology for switched reluctance motors. 20
2.8 The three different states of the converter switches for each phase, magnetization, free-wheeling and de-magnetization. . . 20
2.9 This image schematically illustrates the principle of direct instantaneous torque control [3]. 21
3.1 An example of Modelica code. The code is a trimmed version of the Modelica formulation of the dynamics in (5.22). 24
3.2 An example of Optimica code. This code corresponds to (5.22) minus the dynamic equations which are covered by 3.1. 25
4.1 Novel designs of switched reluctance motors, (left) segmented SRM [4], (middle) circular segmented SRM [5] and (right) axial flux segmented SRM [6]. 29
4.2 Novel designs of switched reluctance motors, (left) L-core SRM [7], (middle) E-core SRM [7], (right) Double Stator SRM [8]. . 29
4.3 Novel designs of switched reluctance motors, (left) π-core SRM [9], (middle) π^2-core SRM [9], (right) Disc SRM [10]. 30
4.4 (left) The two-dimensional geometry of the Comsol model used for the simulation. (right) The flux distribution in the iron core with two phases excited, the current density is plotted in the stator slots. The left color legend is the current density in $\mathrm{A/m^2}$ and the right is the magnetic flux density in T. 31
4.5 The motor characteristics obtained from simulations in Comsol Multiphysics superimposed on those presented in [4]. Solid blue line - Comsol results, dashed black line - simulation results in [4], solid black line - experimental results in [4]. 31
5.1 This plot shows $\partial B/\partial\theta$ and $\partial B/\partial\psi$ in a quarter of a segmented SRM for the specific values $\theta = 4\,\mathrm{deg}$, $i = 6\,\mathrm{A}$. The "warmer" the color, the more does the magnetic field change, corresponding to greater iron losses. 35

5.2 The functions 5.9 as a function of current. The different curves are for different θ-values spaced 2° apart. 36
5.3 The magnitude of the terms in 5.8 at $u = 400\,\mathrm{V}$ and $\omega = 100\,\mathrm{rad/s}$, as a function of current. The different curves are for different θ-values spaced 2° apart. 36
5.4 Comparison between $h_{\omega\omega}(\theta, i)$ and $0.0028\psi(\theta, i)^2$. 37
5.5 Electromagnetic model (blue curve) fitted to the results of the finite elements simulations (black crosses). The right curve shows the flux linkage for five different angles and the right plot shows the torque curves for 5 currents spaced 6 A apart. . . . 38
5.6 Mechanical loss(friction and windage) as a function of velocity for the assumed parameters. 39
5.7 As the temperature of electric motors rise above 200 °C the life time of the insulation materials is reduced. 40
6.1 Copper loss plotted as a function of torque ripple for the results in table 6.1. 46
6.2 Waveforms corresponding to line 1 in table 6.1 (On/Off Control). 46
6.3 Waveforms corresponding to line 2 in table 6.1 ($\alpha_{\mathrm{smooth}} = 0$). . 47
6.4 Waveforms corresponding to line 5 in table 6.1 ($\alpha_{\mathrm{smooth}} = 2$). . 47
6.5 Waveforms corresponding to line 8 in table 6.1 ($\alpha_{\mathrm{smooth}} = 15$). 48
6.6 Waveforms corresponding to line 13 in table 6.1 ($\alpha_{\mathrm{smooth}} = 1000$). 48
6.7 Waveforms corresponding to line 14 in table 6.1 (DITC). . . . 49
6.8 Copper loss plotted as a function of torque ripple for the results in table 6.2. 50
6.9 Typical phase trajectories at a high load torque when torque ripple is penalized. Note how the currents never goes to zero even though negative torque is produced. 51
6.10 Copper loss plotted as a function of torque ripple for the results in table 6.3. 52
6.11 Waveforms corresponding to line 1 in table 6.4 (no current limit). 53
6.12 Waveforms corresponding to line 3 in table 6.1 ($I_{\max} = 9\,\mathrm{A}$). . 54
6.13 Comparison of torque profiles, phase flux linkage profiles and current profiles optimized with respect to just copper losses (dash dotted line) and a complete loss model (solid line). The two cases correspond to the first and last lines of table 6.6. . . 56
6.14 Trajectories optimized with respect to a complete loss model. . 57
6.15 Trajectories optimized with respect to a quadratic penalty on the total torque. 58
7.1 Partial derivatives of the torque τ_k with respect to ψ_k and θ. . 60
7.2 The copper losses as a function of the torque for different angles θ. 60

1. Introduction

1.1 Background

In the 1970's and 1980's scientists discovered that alloys containing the rare-earth metals Samarium and Neodymium could be used to manufacture magnets that produce much stronger magnetic fields than traditional ferrite magnets.

The rare earth permanent magnets were soon after their invention used for making high-performance electric motors, eliminating the need for external excitation, hence boosting the efficiency and power density. These motors have ever since been the preferred choice in demanding engineering applications such as motion control, robotics and electric vehicles where high torque density, high efficiency and variable speed capability are required.

However, with a growing demand and certain countries' recently introduced export restrictions, the prices of Neodymium and Samarium have sky-rocketed, significantly impacting the cost of rare-earth permanent magnet motors.

These recent turns of events have spurred an interest in motor types that do not rely on rare-earth metals.

This thesis will be concerned with one of these motor types, the switched reluctance motor.

Switched Reluctance Motors

Although being similar in principle to the first electric motors constructed in the 1840's, the development of switched reluctance started to gain momentum relatively recently, in the 1980's, due to the following developments in industry [11],

- Power transistors permitted the construction of current regulators switching the current among the phases.
- Development of digital electronics and microprocessors permitting the somewhat more complex control algorithms required for SRMs.
- Development of computers for finite element simulations of SRMs.
- An increased demand for variable-speed electric motors and motion control systems.

The principle and design of the switched reluctance motors will be explained in greater detail in chapter 2 but an example of a typical SRM is shown in figure 1.1.

Switched reluctance motors typically have many distinguished characteristics, both positive and negative. It has a rugged mechanical design, it can be produced at a low cost, it is relatively efficient, inherently fault tolerant, and has a high overdrive capacity. The downsides are that it has a low torque density compared to permanent magnet motors and due to its torque production mechanism it is typically produces a lot of acoustic noise. Unless measures are taken it also exhibits a lot of torque-ripple although this issue can be mitigated at the cost of a reduced efficiency.

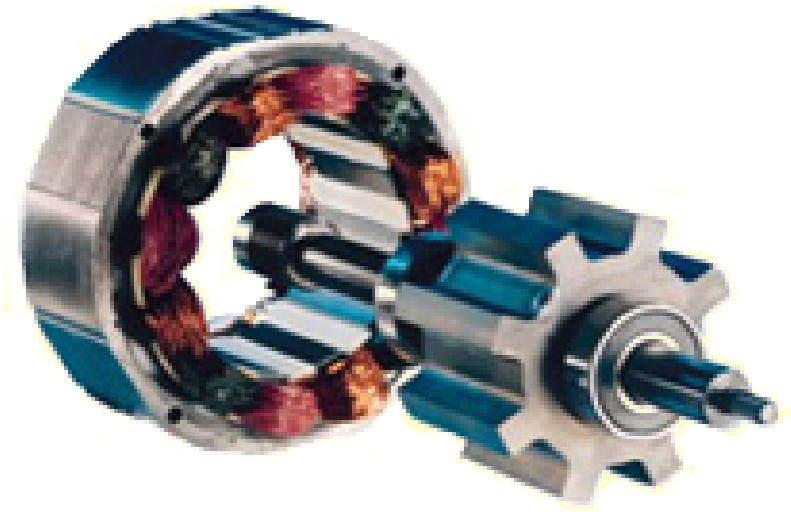

Figure 1.1: The stator and rotor of an SRM used for a washing machine application [1].

As of today switched reluctance machines have still not made a breakthrough in industry. However they seem so have relatively bright future as generators for energy systems, in domestic appliances, and in automotive and aerospace applications [12].

1.2 Problem formulation and objective

There are many desirable features for an electric motor drive system,

- **High peak torque**, the maximal torque that can be delivered by the motor, even if just for a short period of time.
- **High rated torque**, the maximal torque that can be delivered continuously without overheating the motor.
- **Low torque ripple**, a measure of how much the torque output fluctuates, often defined as $(T_{\max} - T_{\min})/T_{\text{average}}$
- **High rated speed**, a high rated speed, i.e. the speed up to which the motor can deliver its rated torque.
- **Quiet operation.**
- **High Efficiency.**
- **Low maintenance.**
- **Low production cost.**
- **Robustness.**

Trade-offs between these have to be made in the design of the motor, the power electronics and the control algorithm. How these trade-offs should be made in an optimal way is non-trivial and depends on the load, operation environment and operation conditions of the motor [13].

This is the problem that the work behind this thesis has been concerned with. Specifically the following research problem has been addressed,

> *"To design a switched reluctance motor system, i.e. both the hardware and the control algorithm, with a performance comparable to that of a permanent magnet motor and a production cost that is significantly lower."*

This is admittedly a hard problem, mainly because it requires deep-domain knowledge about electromechanical machinery, power electronics and control algorithms. In all these areas design-decisions and trade-offs have to be made. Traditionally within the motor industry the development work in these areas has been done relatively independently, inevitably leading to a more or less suboptimal final solution.

The solution to this problem is believed to be a more tightly integrated and automated design process known as co-design, where the hardware and software is designed and optimized simultaneously.

To develop a co-design process for electric motors is a significant project and the scope of this thesis has been more modest,

1. Find a switched reluctance motor design with sufficiently high torque density.

2. Investigate how optimal trade-offs can be made between different control objectives and compare the results to currently used control algorithms.

1.3 Main Results

Through a thorough literature review an SRM design [4, 14] was found that could deliver up to 75 % of the torque of a permanent magnet machine given the same machine size. Finite element simulations were made that verified the machine characteristics claimed in the papers.

A detailed model of the switched reluctance motor model was built in the modeling language Modelica. Based on the model, optimal phase trajectories with respect to different objectives were computed with JModelica. The optimal performance was compared to conventional control approaches and it was found that it was possible to make trade-offs between control objectives such as efficiency and torque ripple.

The optimal control formulation made it possible to use a more detailed loss model as well as removing constraints on the phase currents.

By taking the nonlinear nature of the SRM into account it was possible to compute optimal point-to-point trajectories that significantly reduced the energy spent compared to trajectories computed based on a simplified model. However it should be noted that there were severe torque fluctuations for the optimal trajectory.

The main advantage of the implemented trajectory optimization scheme is that it makes it possible to see how optimal trade-offs in the control design affect the final machine performance.

As for the question of whether a switched reluctance motor system can compete with a rare earth permanent magnet motor it essentially boils down to if a slightly decreased efficiency and lower torque density are offset by a significantly lower price. In some cases the answer could be yes.

1.4 Overview of the Thesis

Chapter 2, Background on switched reluctance motors Terminology is introduced and the characteristics of switched reluctance motors are described.

Chapter 3, Background on optimal control and modeling tools Short introductions to optimal control the computer tools used in the thesis.

Chapter 4, Selecting a high torque density SRM Several recently presented SRM topologies claimed to have a high torque density are briefly reviewed as well as different ways to obtain higher torque through the mechanical design. The performance of the most promising topology is verified through finite element simulations.

Chapter 5, Formulation of the optimal control problem The dynamics and losses in SRMs are discussed and based on this an optimal control problem is formulated.

Chapter 6, Experiments and Results Results from experiments are presented to highlight the main features and advantages of the optimally computed trajectories.

Chapter 7, Problem Structure So remarks on the structure of the optimal control problem, if strong assumptions are imposed it turns out that the problem becomes almost convex.

Chapter 8, Conclusion

Chapter 9, Outlook and future work

2. Background on Switched Reluctance Motors

2.1 Introduction

Some Terminology

An electromechanical device which converts electric energy to mechanical energy is called an electric motor. A device that converts mechanical energy to electric energy is called a generator. Note that often the same device can be used for both purposes.

In a rotating electric machine the part that moves is called the rotor and the part that is stationary is called the stator.

A motor whose electromechanical energy conversion is based on the tendency of its movable parts to move to a position where the reluctance of the applied magnetic field is minimized is called a reluctance motor. In a *switched* reluctance motor the currents are switched between the different phases to keep the rotor in constant motion towards a position of minimum reluctance [11].

An Analogy

The above definition may seem complicated so an analogy (illustrated in fig 2.1) is in place. Note that the analogy is not perfect since a compass needle is magnetized and produces its own magnetic field unlike the rotor of the SRM.

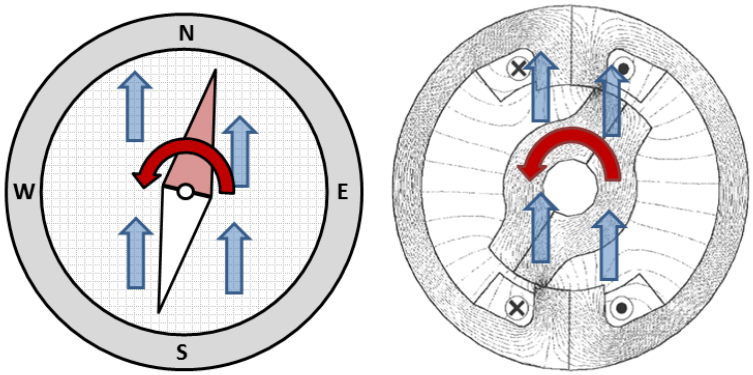

Figure 2.1: The needle of a compass and the rotor of the switched reluctance motor has the same tendency to align itself with the stream lines of the magnetic field that they are subjected to.

As may be readily observed the needle of a compass has a tendency to align itself with the flux lines of earth's magnetic field in order to minimize its potential magnetic energy. This is the same reason that the rotor of the switched reluctance motor has a tendency to align itself with the magnetic field induced by the currents of the active phases.

If the compass is approached by a permanent magnet the direction of the magnetic field in the compass will change and the compass needle will rotate

to a new position of minimal magnetic energy. Likewise, as the currents in the SRM are switched to the next set of phase windings the rotor will have a new minimum of potential energy and torque will be generated by its tendency to move towards that position.

2.2 Basic SRM Concepts

A simple 1-phase SRM can be seen in figure 2.2. In the same figure the aligned and unaligned positions with respect to a given phase are shown. As mentioned above the rotor has a tendency to move from the unaligned to the aligned position in order to minimize the reluctance of the magnetic field.

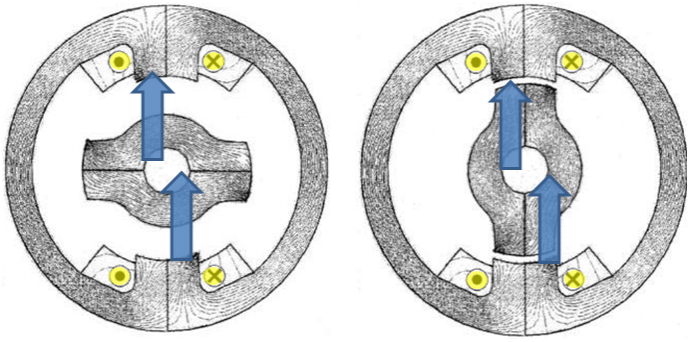

Figure 2.2: The unaligned (left) and aligned rotor (right) positions for a 1-phase SRM [2].

A visualization of the operation of a 2-phase SRM is shown in figure 2.3.

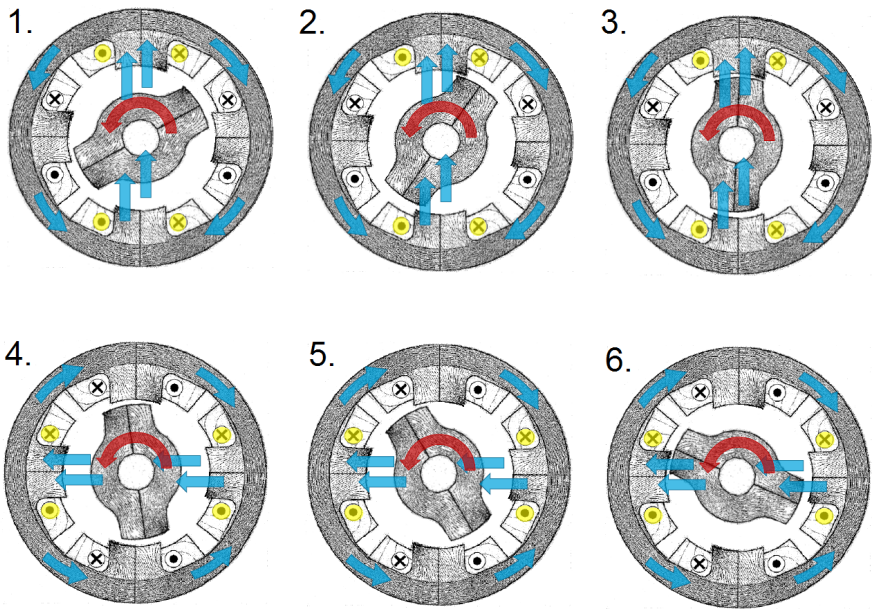

Figure 2.3: In images 1-3 it is seen how the rotor aligns itself with the energized phase to minimize the reluctance of the magnetic field. As the rotor has aligned itself with the active phase it is turned off and the next phase is turned on in order to keep the rotor in rotation as seen in figure 4-6.

2.3 Generic Electrical Drive

A standard drive configuration is shown in figure 2.4. The controller typically gets a torque or speed reference from a higher level computer system. Based on the measured signals, which might be the phase currents, the DC-link voltage, the angular position or the velocity, the controller decides which converter switches that should be closed in order for the motor to track the reference.

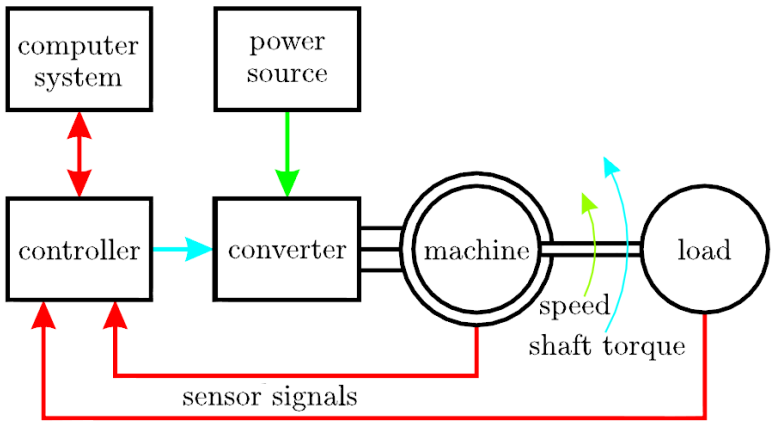

Figure 2.4: A generic schematic of an electric motor drive system [2].

2.4 Energy Conversion Principle

To get a physically correct model of the SRM where energy is conserved, it is necessary to derive a relationship between the so called flux linkage and the generated torque. The equations are common to other electric motors and they may be derived through an energy balance equation [2].

Start by defining the flux-linkage ψ_k for each phase as the amount of flux Φ_k through the phase winding times the number of turns N in the winding,

$$\psi_k := N\Phi_k. \tag{2.1}$$

In most of the literature it is assumed that the phases are magnetically decoupled, i.e. the current in phase winding j does not affect the flux through phase $k \neq j$. That is also done here and hence the subscripts are dropped.

Iron and copper losses have an impact on the machine performance but do not have much influence on the energy conversion principle per se and will hence be ignored in this section.

Faraday's law gives a relation between the applied voltage u and the flux-linkage,

$$u = \frac{d\psi(\theta, i)}{dt}. \tag{2.2}$$

A small amount of electric input energy dW_{in} to the motor may now be expressed

$$dW_{\text{in}} = ui\,dt = \frac{d\psi(\theta, i)}{dt} i\,dt \tag{2.3}$$

$$= \Big(\frac{\partial\psi}{\partial i}\frac{\partial i}{\partial t}\,dt + \frac{\partial\psi}{\partial\theta}\frac{\partial\theta}{\partial t}\Big) i\,dt = i\frac{\partial\psi}{\partial i}\,di + i\frac{\partial\psi}{\partial\theta}\,d\theta. \tag{2.4}$$

Another expression for dW_{in} is obtained by noting that that the electric input energy is converted to magnetic air-gap energy dW_{f} and kinetic energy $\tau(\theta, i)\, d\theta$,

$$dW_{\text{in}} = dW_{\text{f}} + \tau(\theta, i)\, d\theta = \frac{\partial W_{\text{f}}}{\partial i}\, di + \frac{\partial W_{\text{f}}}{\partial \theta}\, d\theta + \tau(\theta, i)\, d\theta. \tag{2.5}$$

Equating 2.3 and 2.5 and identifying the coefficients of the differentials $d\theta$ and di gives

$$\frac{\partial W_{\text{f}}}{\partial i} = i\frac{\partial \psi}{\partial i} \tag{2.6}$$

$$\tau(\theta, i) = i\frac{\partial \psi}{\partial \theta} - \frac{\partial W_{\text{f}}}{\partial \theta}. \tag{2.7}$$

Integrating (2.6) the first expression with respect to i gives

$$W_{\text{f}} = \int_0^i i' \frac{\partial \psi(\theta, i')}{\partial i} di' = \int_0^\psi i(\theta, \psi') d\psi'. \tag{2.8}$$

The magnetic energy W_{f} corresponds to the purple area in figure 2.5. To simplify the expression (2.7) the *co-energy* is usually introduced as $W'_{\text{f}} = i\psi - W_{\text{f}}$, which corresponds to the green area in figure 2.5. From the same figure it is seen that

$$W'_{\text{f}} = \int_0^i \psi di. \tag{2.9}$$

Now (2.7) may be written

$$\tau = \frac{\partial}{\partial \theta} W'_{\text{f}} = \frac{\partial}{\partial \theta} \int_0^i \psi\, di. \tag{2.10}$$

The important equations are (2.2) that implicitly describes the current dynamics and (2.10) that gives the relation between the torque and flux linkage.

Typical curves for the torque and flux linkage of an SRM phase are shown in figure 2.6. Note the nonlinearity of the flux linkage curve in the aligned position that is due to magnetic saturation.

2.5 Converter Topology

There is an overwhelming amount of proposed converter topologies for SRMs, see [15] for an overview. The converter permitting the most flexibility in terms of control is the asymmetric half-bridge converter shown in figure 2.7. This also seems to be the converter of choice in papers considering different control schemes and hence it will be used in this thesis as well.

It is assumed that a constant DC-link voltage is available either off the grid or from a rectifier. In parallel with the DC-supply there is a DC-link capacitor used to recover the magnetic energy when the phase windings are demagnetized. For each phase winding there are two switches, usually insulated gate bipolar transistors(IGBTs) and two diodes.

The asymmetric half-bridge topology permits three different modes of operation (figure 2.8). The three modes may be conveniently and intuitively labeled $-1, 0, 1$ as done in [16].

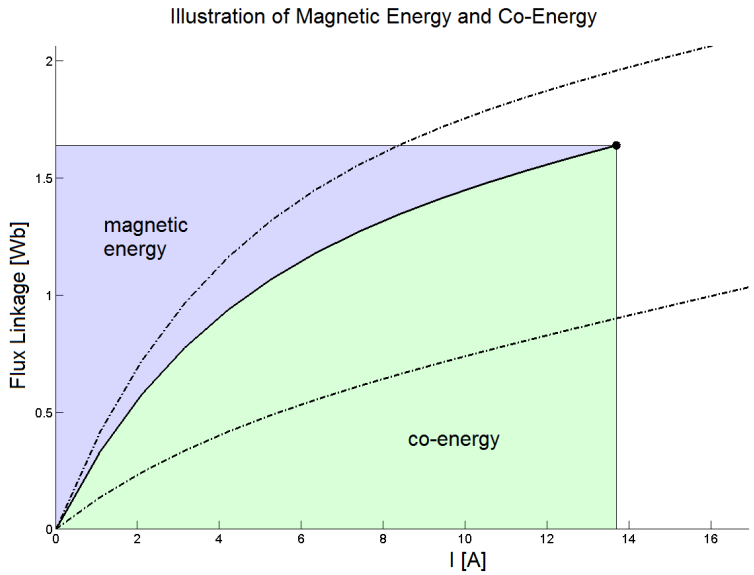

Figure 2.5: The magnetic energy and co-energy for a certain angle and a certain phase current correspond to the colored areas in the figure.

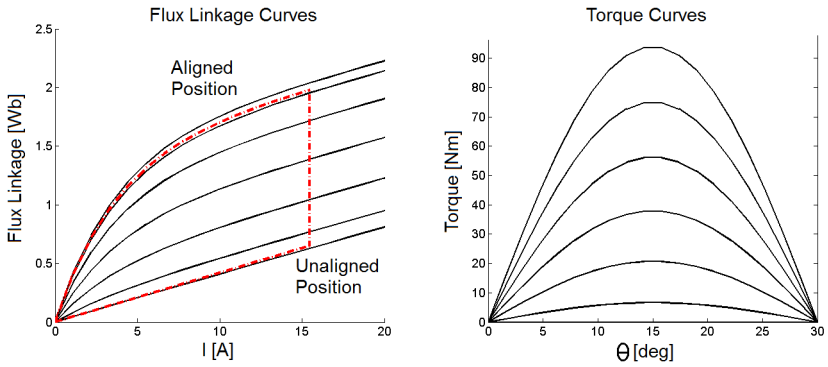

Figure 2.6: Typical flux linkage and torque curves for SRMs.

- 1, Magnetization, both switches are closed and a positive voltage is applied over the phase winding. Input energy is transferred from the power supply to rotational energy and air-gap energy.
- 0, Free-wheeling, one switch is closed and one switch is open. The power supply is disconnected from the motor and energy stored in the air-gap is transferred to rotational energy.
- -1, De-magnetization, both switches are open and the current in the winding flows back to the DC-link capacitor. The air-gap energy is transferred to the load as well as to the supply.

2.6 Control of SRMs

Due to the nonlinear dynamics of switched reluctance motors their control is not as straight forward as for more traditional motors. The different control approaches presented in the literature either try to eliminate the torque-ripple

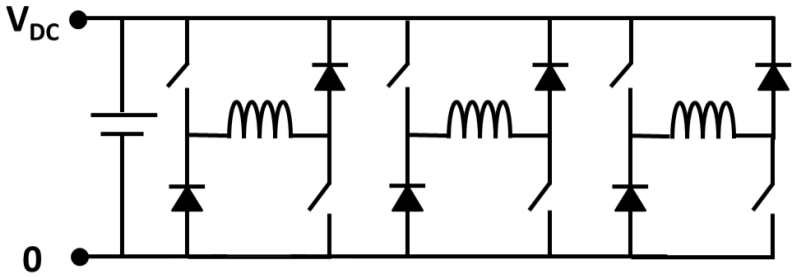

Figure 2.7: The asymmetric half bridge converter, the most common converter topology for switched reluctance motors.

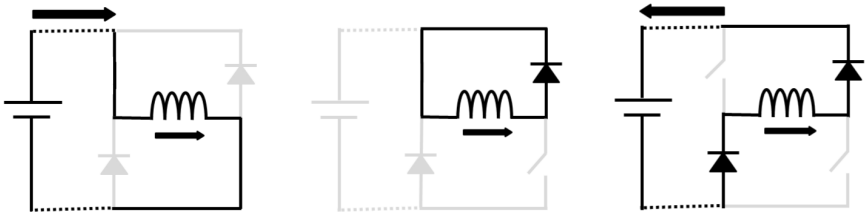

Figure 2.8: The three different states of the converter switches for each phase, magnetization, free-wheeling and de-magnetization.

or increase the efficiency. See [17] for an overview. Two of the most popular options are discussed below.

The first of these control schemes simply tries to increase the efficiency without consideration of torque ripple. The second controller tries to keep a constant torque output as its primary objective and only as a secondary objective minimize the losses. There has been no attempts to make trade-offs between these two objectives.

On/Off Control

The easiest way to get the SRM to produce torque is to simply turn on the current once the rotor reaches a predefined angle, called the turn-on angle and then let the current rise to some prescribed value, keep it constant, and then turn it off at some other prescribed angle, the turn-off angle, which should be close to the aligned position. A typical current/flux linkage-trajectory for this type of control is shown as the red loop in the left part of figure 2.6. The area enclosed by the loop corresponds to the electrical energy converted to mechanical energy.

Direct Instantaneous Torque Control

Direct instantaneous torque control (DITC) [18] is a relatively simple but very efficient method to track a command torque. Its operation is shown schematically in figure 2.9. The idea is basically to keep the estimated torque within some hysteresis thresholds by directly actuating the converter switches.

The DITC approach gives a fast torque response while significantly reducing the amount of switches made in the converter, hence lowering the switching losses compared to using torque sharing functions.

A more recent paper [19] improves on the results in [18] by incorporating

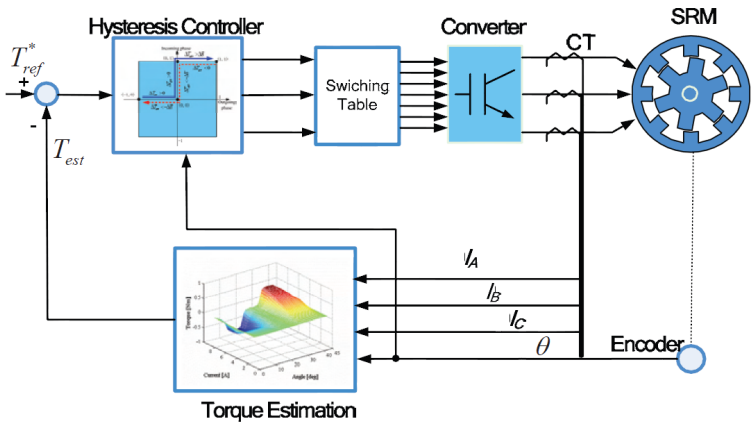

Figure 2.9: This image schematically illustrates the principle of direct instantaneous torque control [3].

a strategy to minimize the copper losses. This is what could be considered the current state of the art in control of SRMs.

Another promising control approach is described in [20] where a model predictive controller with a two sample control horizon is evaluated through simulations.

3. Background on Optimal Control and Modeling Tools

The main content of this thesis is the formulation and solution of an optimal control problem. In this chapter it is described what an optimal control problem is and then the tools and modeling languages used to solve the optimal control problem formulated in this thesis are introduced.

3.1 Optimal Control

Optimal control is the problem of finding a control signal $u(t)$ that minimizes a cost functional

$$\Psi\big[x(t), t_f\big] + \int_{t_0}^{t_f} \mathcal{L}[x(t), u(t), t]dt, \tag{3.1a}$$

where the control signal $u(t)$ and the state $x(t)$ are subject to the differential constraints

$$\dot{x} = f(x(t), u(t), t), \tag{3.1b}$$

the path constraints

$$g(x(t), u(t), t) \leq 0, \tag{3.1c}$$

and the boundary conditions

$$\psi(x_{t_0}, t_0, x_{t_f}, t_f) = 0. \tag{3.1d}$$

In a more general formulation the ordinary differential equation (3.1b) is replaced by a differential algebraic equation $F(\dot{x}, x, t) = 0$. That actually is the formulation that will be used for specifying the optimal control problems in this thesis.

A considerably more thorough treatment of optimal control is given in [21].

3.2 Collocation

In order to solve an optimal control problem in practice it is necessary to rely on numerical algorithms. Among the most popular approaches are the so-called collocation methods where the states $x(t)$ and the control signal $u(t)$ are approximated by piecewise polynomials with node points $t_0 < t_1 < \ldots < t_{n_e} = t_f$. The intervals $[t_k, t_{k+1}]$ are called elements and n_e is the total number of elements used in the collocation.

Discretizing (3.1a) through (3.1d) according to the discretizations of $x(t)$ and $u(t)$ yields a typically large nonlinear program (NLP). The NLP may be solved using standard software and if a solution is found it gives a discretized version of the optimal control signal $u(t)$.

3.3 Modelica

Modelica is a domain-neutral, object-oriented and declarative modeling language designed for the modeling of complex systems [22].

Especially the declarative feature is very useful to the capture the bidirectional energy flows between the electric power source, the magnetic reservoir and the kinetic energy stored in the motor inertia. For example the equation

$$u - Ri = \frac{d\psi}{dt}. \tag{3.2}$$

together with an analytic expression for ψ, will implicitly determine di/dt. This should be contrasted to more standard modeling languages where it is necessary to explicitly express the time derivative of i,

$$\frac{di}{dt} = \frac{v - Ri - [\partial\psi/\partial\theta]\omega}{\partial\psi/\partial i} \tag{3.3}$$

and where the partial derivatives have to be given by explicit formulae.

An example of what the Modelica code look like is shown in figure 3.1.

```
model SRM_dynamics
  extends SRM_parameters;

  // Position and velocity states
  Real theta(start = theta_0,fixed=true) "Angular Position";
  Real omega(start = omega_0,fixed=true) "Angular Velocity";
  Real torqueTotal "Total torque";

  Real[noPhases] I (each free=true) "Phase currents";
  Real[noPhases] torque "Phase toruqes";
  Real[noPhases] psi "Phase fluxes";

  input Real[noPhases] mu (each free=true) "Duty cycle of
      swithces";

equation
  for k in 1:noPhases loop
    // Flux linkage and torque expression
    psi[k] = Lq*I[k] + (A*(1 - exp(-I[k]*B))...;
    torque[k] = ((Ldsat - Lq)*I[k].^2/2 + A*I[k]...;

    // Voltage equation
    V_dc * mu[k] - R*I[k]= der(psi[k]);
  end for;

  // Mechanical equations
  torqueTotal = torque[1] + torque[2] + torque[3] - torqueLoad
      - friction_c*omega - friction_d;
  der(theta) = omega;
  der(omega) = torqueTotal/J;
end SRM_dynamics;
```

Figure 3.1: An example of Modelica code. The code is a trimmed version of the Modelica formulation of the dynamics in (5.22).

3.4 Optimica

Optimica is an extension of the Modelica language which makes it possible to formulate optimal control problems based on Modelica models by specifying constraints and an objective function [23].

An example of Optimica code is shown in figure 3.2.

```
optimization SRM_optimziation (objective = cost(finalTime),
  startTime = 0, finalTime = t_f)
  extends SRM_dynamics;
  Real cost(start=0,fixed=true) "Cost function";
equation
  der(cost) = R*(I[1]^2 + I[2]^2 + I[3]^2);
constraint
  // Boundary conditions
  theta(finalTime) = theta_f;
  omega(finalTime) = omega_f;

  for k in 1:noPhases loop
    // Enforcing converter switch limits
    mu[k] <= 1;
    mu[k] >= -1;

    // Current limits
    I[k] <= I_max;
    I[k] >= 0;

    // Boundary conditions
    I[k](finalTime) = I[k](0);
    mu[k](finalTime) = mu[k](0);
  end for;
end SRM_optimziation;
```

Figure 3.2: An example of Optimica code. This code corresponds to (5.22) minus the dynamic equations which are covered by 3.1.

3.5 JModelica.org

JModelica.org is an extensible Modelica-based open source platform for optimization, simulation and analysis of complex dynamic systems [23]. The platform permits convenient simulation of Modelica models and the solution of optimal control problems through collocation methods. The simulation and optimization features are accessed through a Python interface.

4. High Torque Density Switched Reluctance Motor Options

As the conventional SRM typically has a relatively low torque density a literature review was made of approaches of how it could be increased. This literature review is summarized in this chapter. First two relatively straight-forward ideas related to the materials and manufacturing are mentioned. Thereafter nine recently reported SRM designs that are claimed to have an improved torque density are briefly presented. Out of these nine designs, the most promising design, the segmented RM, was selected to be used in the simulations in rest of the thesis. Finite element simulations were made to verify the claimed performance of the segmented SRM.

4.1 Low Loss Materials for Higher Torque Density

The motor performance is very much dependent on the metal material used in the rotor and the stator (collectively known as the core).

In [24] the resulting SRM performance for three different core materials were compared, a general low-loss silicon steel, an amorphous alloy and a material called "Supercore" with low losses and high permeability. It was found that the use of Supercore significantly increased the efficiency compared to the general low-loss steel (95 % vs 89 % efficiency) although the produced torque was somewhat reduced. The amorphous alloy provided an even higher efficiency although it was prohibitively expensive.

In [25] Hasegawa et al. compare two identical SRMs made of non-oriented silicon steel and permendur, which is an alloy of cobalt and iron that has very high saturated flux density and low iron losses. Through experiments they reach the conclusion that the motor made of permendur produced 20% more torque than the motor made of silicon steel.

4.2 Improved Slot-fill Factor

To obtain high efficiencies and torque densities it is important to pack the copper windings tightly in the stator slots. Chiba reports that an increase in slot-fill factor (the relative copper volume in the stator slots) from 0.431 to 0.487 provided a 1 % increase in efficiency [24].

In [12] it is discussed in the context of segmented SRMs how a technology developed by Mitsubishi Electric [26] can be used to individually wind separate stator segments which increases the slot fill factor and hence the efficiency. The increase in slot fill factor in [26] was from 59 % to 70 %.

4.3 High Torque-Density SRM Designs

Over the last ten years a vast and colorful variety of novel SRM designs have been presented in the literature. While their operating principle is still that of a rotor trying to minimize its reluctance in a switched magnetic field, the magnetic flux paths have been modified in order to improve the performance.

Segmented SRM

In 2002 Mecrow et al. [4] (figure 4.1) introduced a switched reluctance motor with a segmented rotor structure which improves the magnetic utilization compared to a conventional SRM since the active air-gap area is essentially doubled. This is the case since in the conventional three phase SRMs only every third stator tooth is utilized in the magnetic circuit when one phase is excited. In the segmented SRM two out of three stator teeth are utilized. Based on experimental results a 41% increase in torque-density over the conventional SRM is reported.

Further work by Mecrow et al. [14, 27] presents an improved version of the segmented SRM with shorter end-windings and increased performance from numerical parameter optimization.

Circular Slotted Segmented SRM

In a paper from 2008 [5] (figure 4.1) Vandana et al. compares a standard SRM, a segmented SRM and a novel circular slotted segmented SRM (CSSSRM) through simulations and conclude that the CSSSRM has twice the torque density of a regular SRM. Compared to the segmented SRM it improved the torque to weight ratio by 27 %.

Axial Flux Segmented SRM

In [6] (figure 4.1) an axial flux segmented SRM is considered. No experimental results are presented but based on simulation results it is concluded that the motor design would be suitable to be used as a motor mounted inside the wheel of electric vehicles.

E- and L-core SRMs

Krishnan et al. has suggested the idea of using E- and L-shaped stator yokes [7] as seen in figure 4.2. In these designs some stator teeth are shared between two phases, meaning shortened the flux paths and reduced mass of iron and copper. This leads to increased efficiency and torque density. The straight angles in the stator in the stator yoke improve the manufacturability.

Double Stator SRM

Abbasian et al. [8] has designed a double stator SRM (figure 4.2) with stators on both the inside an outside of a circular shell rotor. The design tries to circumvent the problem that most of the force developed in a conventional SRM is in the radial direction and does not contribute to produce useful torque but rather acoustic noise. In the paper it is concluded that the novel design offers superior power density to a conventional SRM.

π- and π^2-core SRMs

The π-core SRM [9] (figure 4.3) is designed for in-wheel EV applications and utilizes a segmented stator structure with π-shaped segments in order to min-

imize core losses. Through simulations it is concluded that the novel design increases the average torque by 23 % and reduces the torque ripple by 41 %.

The same authors also propose a dual rotor model based on the same concept which they call the π^2-core SRM and which they claim has the same advantages as the π-core SRM. See figure 4.3 for pictures.

Disc SRM

In [10] a "disc SRM" (figure 4.3) is introduced in which a rotor consisting of a disc with certain areas of high permeability is sandwiched between to stators. Simulation and experimental results show a 10 % increase in torque compared to a conventional SRM.

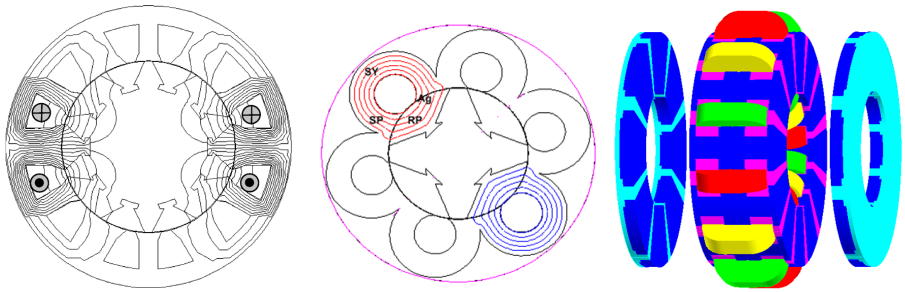

Figure 4.1: Novel designs of switched reluctance motors, (left) segmented SRM [4], (middle) circular segmented SRM [5] and (right) axial flux segmented SRM [6].

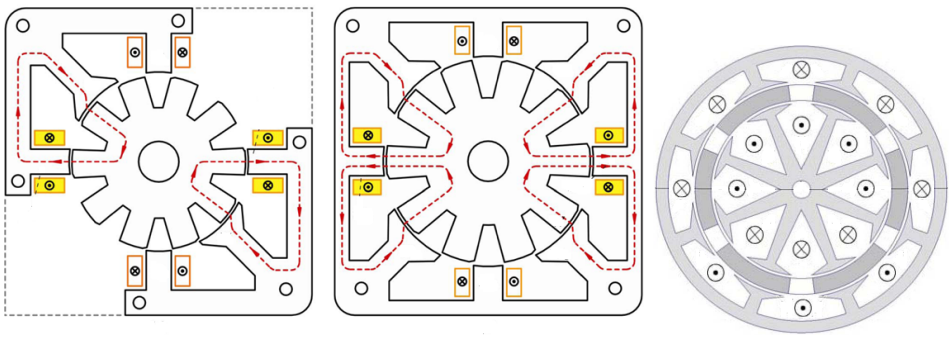

Figure 4.2: Novel designs of switched reluctance motors, (left) L-core SRM [7], (middle) E-core SRM [7], (right) Double Stator SRM [8].

4.4 Selecting a Suitable Switched Reluctance Motor Topology

Given the author's limited knowledge of electric motors it was hard to decide on which of the motor designs in the previous section that had the best potential for motion control applications.

The choice fell on Mecrow's segmented SRM since it had been featured in the most papers [4, 14, 27] and that there seems to be enough belief in the idea to keep up the research for 10 years.

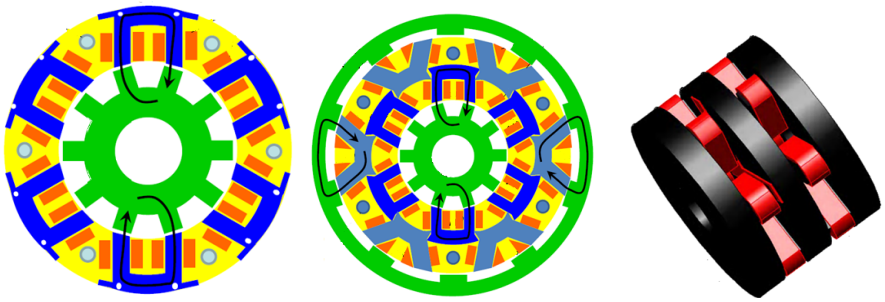

Figure 4.3: Novel designs of switched reluctance motors, (left) π-core SRM [9], (middle) π^2-core SRM [9], (right) Disc SRM [10].

Unlike several of the other mentioned geometries a lot of experimental results are available and also a relatively complete description of the motor design parameters.

It may be observed that the insights on which the segmented SRM are based, that flux paths should be kept short and magnetic utilization high, are not new. TJE Miller mentions in [11] that already in 1833 it had been stated by Rev. William Ritchie, Professor of Natural Philosophy in the University of London that:

> Having constructed, with great pains, an electro-magnet according to the American method, and connected it with a battery, I found it would carry about one hundred and forty pounds. I then rolled about twelve feet of copper ribbon about the middle of the lifter, which weighed about half a pound, and connected the ends of the coil with the same battery, the electromagnet being now used as the lifter, and was surprised to find that the lifter was a more powerful magnet than that which had cost me so much labor to prepare. All that is necessary, then, in making a powerful electro-magnet, is simply to roll a ribbon of copper (metallic contact being prevented by a thin tape interposed) about a short bar of soft iron, and use a short-shoe lifter.

Miller thereafter notes that

> Ritchie's highly significant conclusion that magnetic circuits should be kept short and, by implication, well coupled with the electric circuit, was largely lost on his contemporaries.

Interestingly enough it seems like this conclusion also has been lost on the SRM research community that has pretty much exclusively worked with the conventional SRM design up until the last 10 years.

4.5 The Segmented Switched Reluctance Motor

It should be noted that Mecrow et al. has designed a more recent, single-pitched segmented SRM [14] with certain advantages over the multi-pitched version presented here. The reason that the multi-pitched version was still chosen for the work in this thesis was that that it has a more regular geometry and that its design parameters were available.

Finite Element Simulations Segmented SRM

To verify the performance of the segmented SRM, finite element simulations were made based on the parameters in [4] and the results were compared to those in the paper.

The simulations were carried out in Comsol Multiphysics, a commercial finite elements program. The magnetostatic flux distribution and resulting torque were computed at different angles and phase currents. The simulation model was in 2D and is shown in figure 4.4. Due to symmetry it was sufficient to simulate just a quarter of the full geometry. A typical magnetic flux distribution at a certain angle and phase current is shown in 4.4.

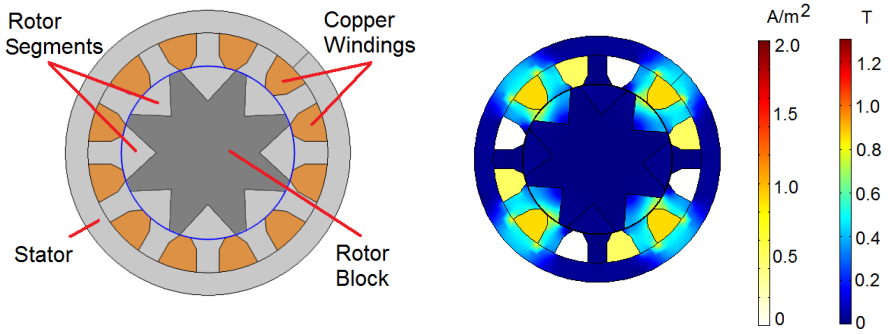

Figure 4.4: (left) The two-dimensional geometry of the Comsol model used for the simulation. (right) The flux distribution in the iron core with two phases excited, the current density is plotted in the stator slots. The left color legend is the current density in A/m^2 and the right is the magnetic flux density in T.

The flux was computed as the flux through the back-iron behind slot of the excited phase. It was not clear from the paper if this is the exactly same quantity that is considered in the reference paper.

A comparison between the obtained simulation results and the results in [4] are shown in figure 4.5. The author believes that the discrepancy between the

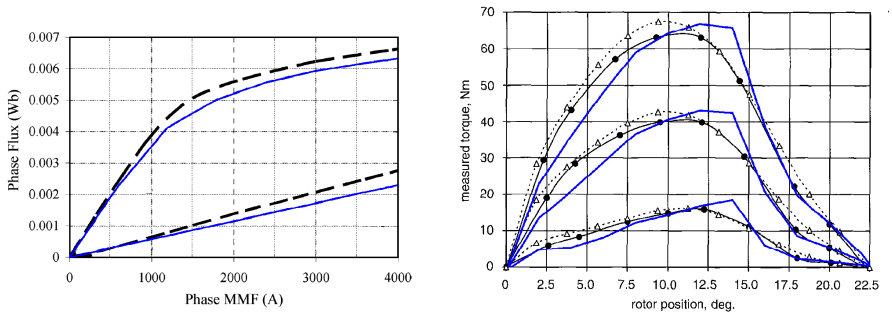

Figure 4.5: The motor characteristics obtained from simulations in Comsol Multiphysics superimposed on those presented in [4]. Solid blue line - Comsol results, dashed black line - simulation results in [4], solid black line - experimental results in [4].

flux-characteristics to a large extent can be explained by that the simulations were carried out in 2D without making any corrections for the end-effects.

5. Formulation of the optimal control problem

In this chapter the dynamics and different losses of the SRM are discussed before they are summarized as an optimal control problem. Typically the copper losses is the dominant loss mechanism followed by iron losses and switching losses, but these figures depend on the operating conditions that motor is optimized with respect to. In [24] the copper and iron losses are roughly equal and in [27] the copper losses are five times larger than the iron losses.

5.1 Copper Loss Modeling

The resistive losses in the windings are modeled by the familiar expression

$$P_{\mathrm{Cu}} = \sum_{k=1}^{3} R i_k^2. \tag{5.1}$$

Also eddy current losses occur in the windings [28], however this effect is both relatively small and also hard to model. Thus it was decided to leave it out of the model.

5.2 Iron Loss Modeling

As the magnetic flux through the iron core of the motor changes, energy will be lost in terms of heat due to a number of different physical processes. These losses are called iron losses and essentially depend on the rate of change of the magnetic field, dB/dt. They thus go up as the speed increases.

The iron losses also depend greatly on the type of steel used in the motor and can make up more than 50 % of the total losses of an SRM [29].

According to [30] the iron losses may be separated into three terms, hysteresis losses, eddy current losses and excess losses. These three different terms and their incorporation into the optimal control problem are explained below.

Eddy Current Losses

As the magnetic field through a material changes, according to Faraday's law $\nabla \times \mathbf{E} = -\partial \mathbf{B}/\partial t$, an electromotive force is induced around loops inside the material. In a conductor these EMFs will give rise to currents which in turn produce resistive losses.

The eddy current losses at a point in the material are given by [31, 32]:

$$P_{\mathrm{eddy}} = \frac{a^2 \sigma}{12} \Big(\frac{dB}{dt} \Big)^2 = C_{\mathrm{eddy}} \Big(\frac{dB}{dt} \Big)^2, \tag{5.2}$$

where σ is the conductivity of the material and a is the thickness of the material perpendicularly to $d\mathbf{B}/dt$.

The dependence of (5.2) on a is the reason that motor cores typically are made of laminated steel.

Hysteresis Losses

Hysteresis losses occur as the microscopic magnetic domains inside the steel change size and reorient themselves. The hysteresis may be modeled as [31,32]:

$$P_{\text{hysteresis}} = f(|B|)\frac{dB}{dt}, \tag{5.3}$$

where f is a nonlinear function depending of the hysteresis curve of the material in question. The two references use different approximations to f, in [31],

$$f(|B|) \approx H_c, \tag{5.4}$$

where H_c is the coercive force of the material. A typical value of H_c for the type of steel used in electric motors is about $30 - 60\,\text{A/m}$ [33]. In the optimization problem H_c was arbitrarily taken to be $40\,\text{A/m}$.

Excess Losses

Eddy currents and hysteresis does not suffice to explain all the iron losses, the residual losses are called excess losses and in [30] it is argued that they are of the form

$$P_{\text{exc}} = C_{\text{exc}}\Big(\frac{dB}{dt}\Big)^{3/2}. \tag{5.5}$$

The excess losses are small compared to the hysteresis and eddy current losses and are not to be included in the optimal control problem.

Iron Loss as a Function of Lumped Quantities

To be able to incorporate the iron losses into the optimal control problem they must be given as a function of the motor states θ, ω, i_k and the input signals u_k.

An attempt to derive a such expression is made in [32]. Some scrutiny of the argument reveals however that the expression used for dB/dt does not depend on the rotational velocity ω which is typical for eddy-current losses. The main error in the assumptions is that the magnetic flux distribution throughout the motor is only dependent on the flux linkage when it in reality is very much dependent on the angle θ as well.

The correct expression for dB/dt (neglecting higher-order effects such as flux diffusion) is

$$\frac{dB}{dt} = \frac{\partial B}{\partial \psi}\frac{d\psi}{dt} + \frac{\partial B}{\partial \theta}\frac{d\theta}{dt} = \frac{\partial B}{\partial \psi}u + \frac{\partial B}{\partial \theta}\omega,$$

where the partial derivatives depend on θ and i.

The total eddy current losses throughout the motor are given by

$$\begin{aligned} p_{\text{eddy}}(\theta, \omega, i, u) &= \frac{\sigma a^2}{12}\int_V \Big(\frac{dB}{dt}\Big)^2 dV && (5.6)\\ &= \frac{\sigma a^2}{12}\int_V \Big(\frac{\partial B}{\partial \psi}\Big)^2 u^2 + 2\frac{\partial B}{\partial \theta}\frac{\partial B}{\partial \psi}u\omega + \Big(\frac{\partial B}{\partial \theta}\Big)^2\omega^2\, dV. && (5.7)\\ &= h_{uu}(\theta, i)u^2 + h_{u\omega}(\theta, i)u\omega + h_{\omega\omega}(\theta, i)\omega^2 && (5.8) \end{aligned}$$

where

$$h_{uu}(\theta, i) = \frac{\sigma a^2}{12} \int_V \left(\frac{\partial B}{\partial \psi}\right)^2 dV \tag{5.9a}$$

$$h_{u\omega}(\theta, i) = \frac{\sigma a^2}{12} \int_V 2\frac{\partial B}{\partial \theta}\frac{\partial B}{\partial \psi}\, dV \tag{5.9b}$$

$$h_{\omega\omega}(\theta, i) = \frac{\sigma a^2}{12} \int_V \left(\frac{\partial B}{\partial \theta}\right)^2 dV. \tag{5.9c}$$

The partial derivatives in (5.9) may be approximated by finite differences $(B(\theta + \Delta\theta, \psi) - B(\theta, \psi)/\Delta\theta)$ and $(B(\theta, \psi + \Delta\psi) - B(\theta, \psi)/\Delta\psi)$. The B-field was calculated in using Comsol Multiphsyics for many different values of θ and i over a 0.6 mm $\times$ 0.6 mm-grid.

A plot of these finite differences for a certain combination of θ and i are shown in figure 5.1.

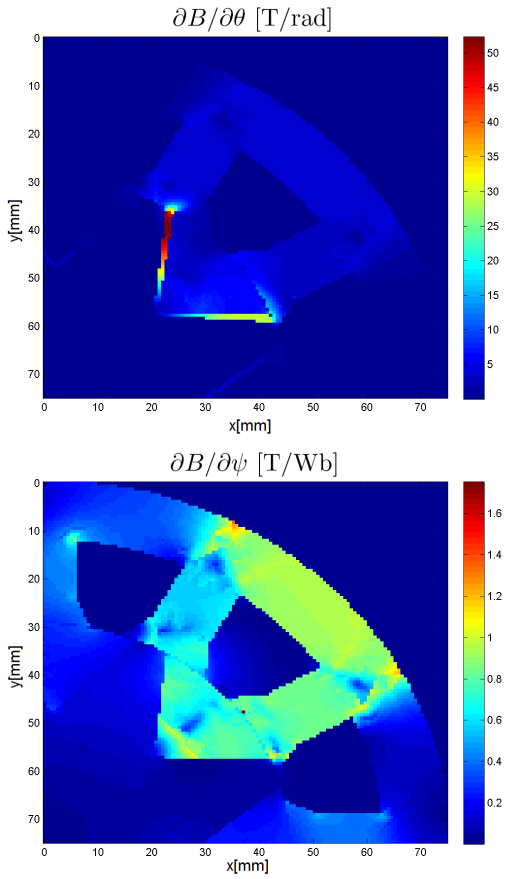

Figure 5.1: This plot shows $\partial B/\partial\theta$ and $\partial B/\partial\psi$ in a quarter of a segmented SRM for the specific values $\theta = 4\,\text{deg}$, $i = 6\,\text{A}$. The "warmer" the color, the more does the magnetic field change, corresponding to greater iron losses.

Given the B-field data, numerical approximation to the integrals (5.9) were computed in MatLab. The computed coefficients as functions of θ and i are shown in figure 5.2.

To get an idea of the relative contributions of the terms in (5.8) they were plotted for values of u and ω corresponding to relatively demanding but reasonable operating conditions, the results are shown in figure (5.3).

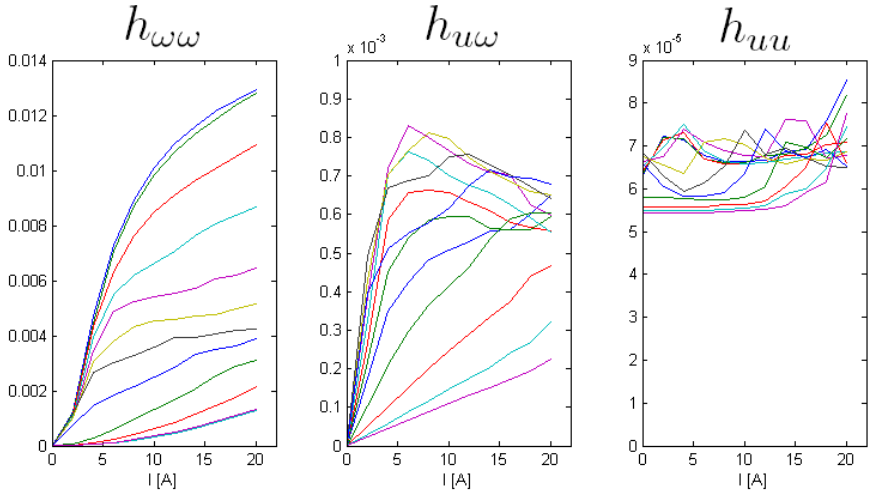

Figure 5.2: The functions 5.9 as a function of current. The different curves are for different θ-values spaced 2° apart.

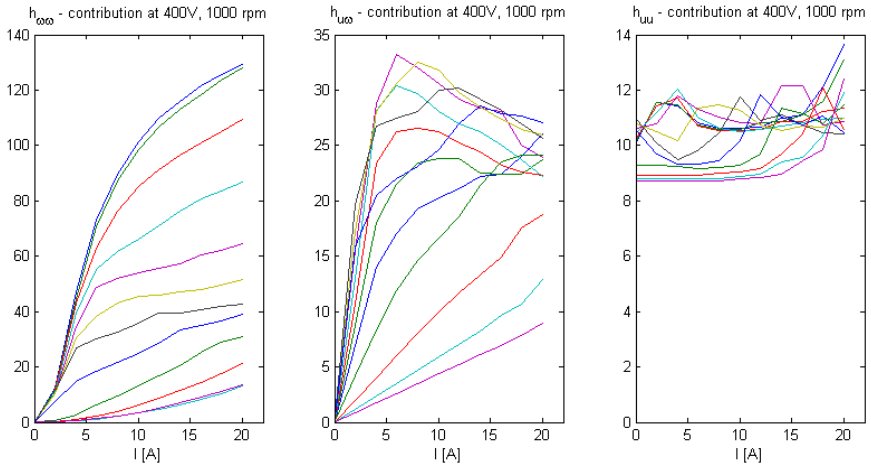

Figure 5.3: The magnitude of the terms in 5.8 at $u = 400\,\mathrm{V}$ and $\omega = 100\,\mathrm{rad/s}$, as a function of current. The different curves are for different θ-values spaced 2° apart.

Since of work in this thesis is mostly qualitative, only the most important term in 5.9, $h_{\omega\omega}(\theta, i)$ was included in the model. It was approximated very crudely by $k_{\mathrm{eddy}}\psi(\theta, i)^2$ as shown in figure 5.4.

The hysteresis losses were in a similar way approximated by $p_{\mathrm{hysteresis}} = k_{\mathrm{hysteresis}}\psi(\theta, i)\omega$ with $k_{\mathrm{hysteresis}} = 0.1\,\mathrm{Ws/Wb}$.

5.3 Converter Modeling

The notation $\tilde{\mu}_k \in \{-1, 0, 1\}$ for the converter states introduced in section 2.5 is not only an intuitive way of labeling the three different converter states but also permits the phase voltage equation (2.2) to be written in the very convenient form

$$\tilde{\mu}_k V_{\mathrm{dc}} = \frac{d\psi}{dt}, \tag{5.10}$$

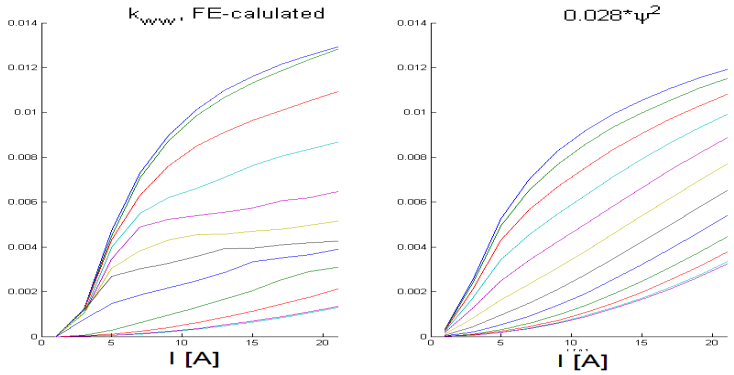

Figure 5.4: Comparison between $h_{\omega\omega}(\theta, i)$ and $0.0028\psi(\theta, i)^2$.

where the three different equations for the electric dynamics, one for each converter state, are summarized into one equation.

To actually solve an optimization problem with discrete inputs $\tilde{\mu}$ would lead to a mixed-integer nonlinear program, which in general are hard to solve efficiently. If $\tilde{\mu}$ instead is replaced by its time-average over some small time interval ΔT,

$$\mu_k \approx \frac{1}{\Delta T} \int_{-\Delta T/2}^{\Delta T/2} \tilde{\mu}_k dt \in [-1,\ 1], \tag{5.11}$$

the resulting continuous optimal control problem can be solved much more efficiently.

The approximation () is accurate for quantities that depend on the integral of the applied voltage such as the flux linkage, torque and copper losses. The eddy currents do depend directly on the applied voltage but since this voltage dependence is not modeled it is not a problem.

Converter Losses

The losses in the inverter consist of conduction losses and switching losses. For a given voltage and switching frequency they are reasonably proportional to the current flowing through them [34],

$$p_{\text{switching}} = k_{\text{switching}}(i_1 + i_2 + i_3). \tag{5.12}$$

Based on data sheets for insulated gate bipolar transistors, the value of $k_{\text{switching}}$ was taken to be $0.9\,\text{W/A}$.

5.4 Electric Equations

Using the approximation (5.3) and taking into account the voltage drop due to the winding resistance, the equation (5.10) may be written

$$\mu_k V_{\text{dc}} - R i_k = \frac{d\psi_k}{dt} \tag{5.13}$$

Analytic Approximations of Torque and Flux Linkage

To be able to formulate the optimal control problem in the Optimica language the electromechanical characteristics in figure 4.5 had to be represented by analytic functions.

There are many examples in the literature of how this can be done, in many cases as a linear combinations of basis functions made up of products of splines and sine factors. In other cases it is assumed that flux linkage can be written as a θ-dependent interpolation between the unaligned and aligned flux linkage curves.

This is done for example in [35] which is the basis for the switched reluctance motor block in the Simulink's SimPowerSystems. This semi-empirical model assumes that there is no saturation in the unaligned position in which case it can be written $\psi(\theta_{\text{unaligned}}, i) = L_q i$ where L_q is the unaligned inductance. For the aligned position an exponentially decaying magnetization is assumed, $\psi(\theta_{\text{aligned}}, i) = L_{\text{dsat}} i + A(1 - e^{-Bi}) - L_q i$ where L_{dsat} is the saturated inductance and A and B are chosen to obtain a good fit to the aligned flux linkage curve. For angles between the unaligned and aligned position the flux linkages are interpolated by a function $f(\theta)$.

$$\psi(\theta, i) = \big[1 - f(\theta)\big] L_q i + f(\theta)\big[L_{\text{dsat}} i + A(1 - e^{-Bi})\big] \tag{5.14}$$

Using (2.10) the torque as a function of θ and i may be obtained,

$$\tau(\theta, i) = \left[\frac{(L_{\text{dsat}} - L_q)^2 i}{2} + Ai - \frac{A(1 - e^{-Bi})}{B}\right] f'(\theta). \tag{5.15}$$

In [35] $f(\theta)$ was chosen to be a third order spline function defined for a quarter of a phase period. To implement it in Modelica for an arbitrary angle would have been complicated.

To avoid these issues and at the same time get a better fit to the finite element data, f was taken to be a fifth order Fourier series with period $2\pi/4$. Fitting the parameters of (5.14) in Matlab, the approximations in figure 5.5 were obtained. The fit is not perfect but captures the nonlinearity due to magnetic saturation and the asymmetry of the torque curves.

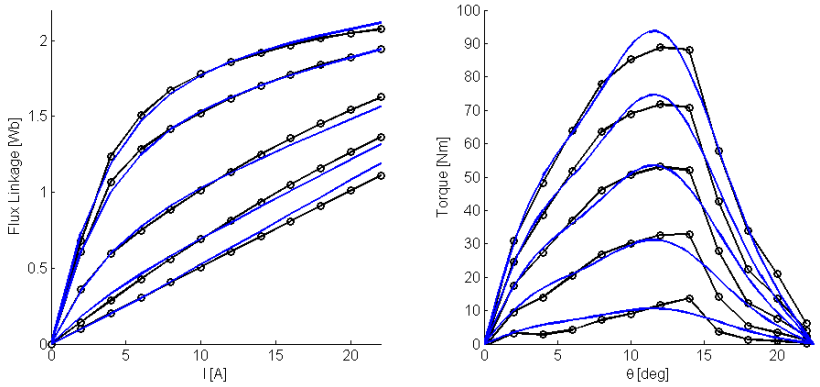

Figure 5.5: Electromagnetic model (blue curve) fitted to the results of the finite elements simulations (black crosses). The right curve shows the flux linkage for five different angles and the right plot shows the torque curves for 5 currents spaced 6 A apart.

5.5 Mechanical Equations

Let the torque produced by phase k be denoted by $\tau_k(\theta, i)$. Since it is assumed that there are no cross couplings between the phases, the total electromechanical torque τ_{el} produced by the machine is given by

$$\tau_{\text{el}} = \tau_1(\theta, i_1) + \tau_2(\theta, i_2) + \tau_3(\theta, i_3). \tag{5.16}$$

Including a load torque τ_{load} and a friction/windage term $\tau_{\text{fw}} = -d\omega - c$ the mechanical equations may be written

$$\dot{\omega} = (\tau_{\text{el}} + \tau_{\text{load}} - d\omega - c)/J \tag{5.17}$$

$$\dot{\theta} = \omega. \tag{5.18}$$

Friction and Windage Losses

There were no data available for the friction and windage losses of the segmented SRM. As the investigation in this this thesis is qualitative in nature these losses are instead estimated.

Based on data for similar machines [12, 32] the coefficients in 5.17 were taken to be $c = 0.1$ Nm and $d = 2{\cdot}10^{-4}$ Nms. The dependence of the mechanical losses on velocity with this choice of parameters are shown in figure 5.6.

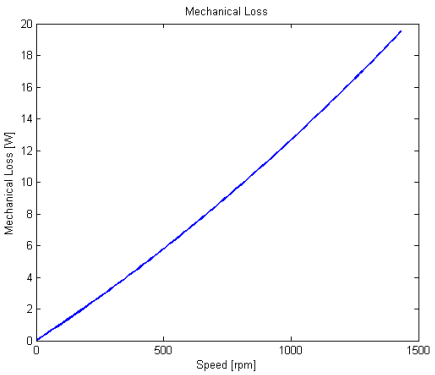

Figure 5.6: Mechanical loss(friction and windage) as a function of velocity for the assumed parameters.

Note that the mechanical losses will have very little influence on the optimal trajectory. For a unidirectional point-to-point movement the total loss contribution from the Coulomb friction term will be the independent of the trajectory and for a fixed final-time problem so will the viscous friction contribution. Only indirectly will these effects influence the trajectory through an increase in the required torque and hence an increase in the required phase currents.

Also note that in (5.17) the Coulomb term should actually be $-\text{sign}(\omega)c$ and that this would require a discontinuity in the dynamic constraints. However as long as it is made sure that the velocity for the resulting optimal trajectory is positive there is no need for this.

5.6 Thermal Modeling

What generally limits the torque and power output of an electric motor of a given size is that its temperature must not get too high. As seen in figure 5.7 the higher the temperature the motor is operating at the more rapidly does the insulation materials deteriorate, eventually leading to a very costly winding failure requiring replacement or rewinding of the motor.

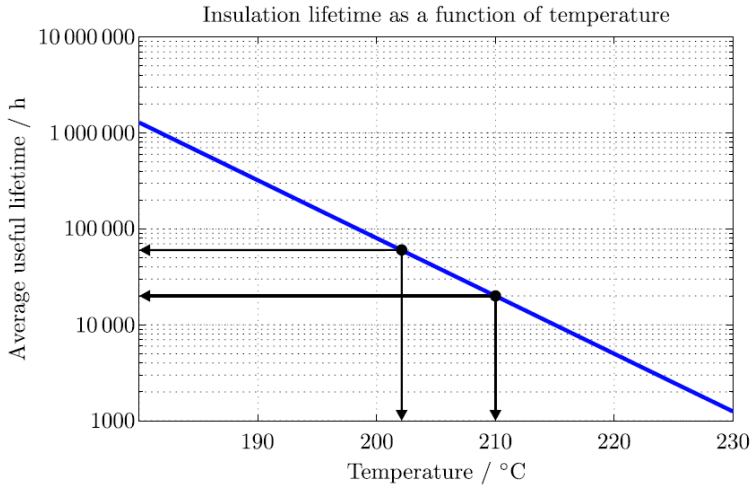

Figure 5.7: As the temperature of electric motors rise above 200 °C the life time of the insulation materials is reduced.

In discussing the limits of direct instantaneous torque control it is stated in [Doncker2003] that

> The thermal capacity and, therefore, the peak converter current are limiting the maximum achievable torque with DITC in the same way as with conventional current profiling techniques.

It is true that the thermal capacity is the limiting factor, however, a limit on the instantaneous currents does not accurately reflect the actual thermal constraints. The motor itself has a thermal time-constant on the order of minutes [36], and even if the inverter has not been dimensioned for overload it should be able to sustain over currents for a couple of tenth of a second.

By using optimal control to design the phase trajectories over some short time interval it is possible to allocate the heat budget over the this entire time interval rather than limiting the instantaneous currents which is necessary for instantaneous torque controllers.

To summarize, it does not make sense to include instantaneous constraints on the currents other than possibly those imposed by the converter capacity. The quantity that has to be limited is instead the average losses but since that quantity is the objective function to be minimized it does not has to be included as a constraint.

5.7 Constraints

The only explicit constraint that have to be imposed are (possibly) current limits depending on the converter rating and velocity constraints imposed by

the mechanical design.

$$0 \leq i_k \leq i_{\max} \qquad k = 1, 2, 3 \tag{5.19}$$

$$-v_{\max} \leq v \leq v_{\max}. \tag{5.20}$$

Given the definition of μ_k the following additional constraints must also be imposed,

$$-1 \leq \mu_k \leq 1. \tag{5.21}$$

5.8 Objective Function

The objective function for the optimal control problem is taken to be the total losses, plus in relevant cases a term penalizing torque ripple,

- Copper losses Ri_k^2
- Friction losses $c|\omega| + \omega^2$
- Eddy current losses $k_{\text{eddy}}\psi_k^2\omega^2$
- Hysteresis losses $k_{\text{hysteresis}}\psi_k\omega$
- Inverter losses $k_{\text{inverter}}|i_k|$
- Penalty on non-smooth torque $\alpha(\tau_{\text{ref}} - \tau_{\text{out}})^2$ or $\alpha(\dot{\tau}_{\text{tot}})^2$.

5.9 Summary of the Optimal Control Problem

Summing up the relevant equations from the above sections gives the following optimal control problem

$$\text{minimize} \int_0^{t_{\text{f}}} \sum_{k=1}^{3} \left(Ri_k^2 + k_{\text{eddy}}\psi_k^2\omega^2 + k_{\text{hysteresis}}\psi_k\omega + k_{\text{inverter}}|i_k| \right. \tag{5.22a}$$

$$\left. c|\omega| + d\omega^2 + \alpha(\tau_{\text{ref}} - \tau_{\text{el}})^2 \right) dt, \tag{5.22b}$$

subject to the following differential constraints

$$\mu_k V_{\text{dc}} - Ri_k = \frac{d\psi_k}{dt} \qquad k = 1, 2, 3 \tag{5.22c}$$

$$\tau_{\text{el}} = \tau_1(\theta, i_1) + \tau_2(\theta, i_2) + \tau_3(\theta, i_3) \tag{5.22d}$$

$$\dot{\omega} = (\tau_{\text{el}} + \tau_{\text{load}} - d\omega - c)/J \tag{5.22e}$$

$$\dot{\theta} = \omega, \tag{5.22f}$$

the following inequality constraints

$$-1 \leq \mu_k \leq 1 \qquad k = 1, 2, 3 \tag{5.22g}$$

$$0 \leq i_k \leq i_{\max} \qquad k = 1, 2, 3 \tag{5.22h}$$

$$-v_{\max} \leq v \leq v_{\max}, \tag{5.22i}$$

and the following boundary constraints,

$$\theta(0) = \theta_0 \qquad \theta(t_f) = \theta_f \tag{5.22j}$$

$$\omega(0) = \omega_0 \qquad \omega(t_f) = \omega_f \tag{5.22k}$$

$$i_k(0) = 0 \qquad k = 1, 2, 3 \tag{5.22l}$$

6. Experiments and Results

To demonstrate the advantages of the trajectories resulting from the optimal control problem they were benchmarked against conventional control approaches. This was done in two different types of test cases, constant velocity operation and point-to-point movements.

6.1 Experiment Procedure

The optimal trajectories were computed using the local collocation algorithm in JModelica. Between 200-500 elements were used, each with 1 collocation point. It was found that the total solution time was significantly sped up if a smaller optimization problem using some 20 elements were solved initially and the computed trajectories used as an initial guess for the problem with the larger number of elements. The solution time for each problem varied between some hundred milliseconds to several minutes depending on the number of elements and the quality of the initial guess.

Typically only copper losses are considered when discussing control of SRMs, consequently this is also done here except in one case, in order to investigate the effects of including iron losses and switching losses.

Note on the Torque Ripple Metric

In the literature the torque ripple is most often defined as the peak to peak torque variation divided by the average torque,

$$\mathrm{TR}_{\mathrm{abs}} = \frac{T_{\max} - T_{\min}}{T_{\mathrm{average}}}. \tag{6.1}$$

However since the penalty term in the objective function was of the form $(T_{\mathrm{ref}} - T(t))^2$ a more relevant measure of torque ripple should the normalized rms value of the deviation from the reference torque,

$$\mathrm{TR}_{\mathrm{rms}} = \frac{\sqrt{\int_0^{t_{\mathrm{f}}} (T_{\mathrm{ref}} - T(t))^2 \, dt}}{T_{\mathrm{average}}}. \tag{6.2}$$

For the trajectories given in this chapter both measures of torque ripple are given. It can be seen that they correlate reasonably well.

6.2 Test Case Type 1: Constant Velocity Operation

In the following test cases the motor was rotating at a constant velocity and the objective was to deliver a certain amount of torque while optimizing some performance criterion. It was assumed that the inertia of the load was large enough that the velocity indeed remained constant even when there were torque fluctuations.

The optimal trajectories were simulated in Simulink and compared to on/off control as well as DITC, these control approaches were briefly described in 2.6.

To have the on/off controller work at its best it is necessary to optimize the turn on and turn off angles. These were found by exhaustively evaluating the torque and copper losses for all combinations of angles on a finely spaced grid.

Also the DITC requires tuning of the turn on and turn off angles to achieve optimal performance although it is not overly sensitive to these. Just a small amount tuning of these angles were made and it is expected that the performance could be somewhat improved by further tuning.

Different experiments were made to highlight the advantages of using a complete SRM model of the dynamics and losses compared to less complex control approaches. The following things were investigated,

- **Trade-off between copper loss and torque ripple**, by adding a term $\alpha_{\text{smooth}}(\tau_{\text{ref}} - \tau(t))^2$ it was possible to penalize the deviation from the reference torque. It was investigated how different values of α_{smooth} affected the copper losses and torque ripple in different operating regions. See figures 6.1 through 6.10.
- **Current limits**, by allocating the phase torques and phase currents over an entire phase period it is possible to guarantee the thermal constraints without imposing limits on the phase currents. It is shown in experiments that the current limits actually increase the losses and hence lead to increased motor temperatures. See figures 6.11 and 6.12.
- **Inclusion of iron losses**, by including the iron losses into the objective function it was possible to get a better chance to minimize the total losses. See figure 6.13.

Optimal Control Formulation

In formulating the optimal control problem for constant velocity operation it was possible to exploit the cyclic nature of the SRM dynamics and just do the optimization over a third of a phase period, i.e. $\pi/12$ radians. More precisely the following boundary conditions were imposed for a given angular velocity ω_0,

$$t_{\text{f}} = pi/12/\omega_0 \tag{6.3a}$$

$$\theta(0) = 0 \qquad \theta(t_{\text{f}}) = \pi/12 \tag{6.3b}$$

$$\omega(t_{\text{f}}) = \omega_0 \tag{6.3c}$$

$$i_2(0) = i_1(t_{\text{f}}) \qquad i_3(0) = i_2(t_{\text{f}}) \qquad i_1(0) = i_3(t_{\text{f}}) \tag{6.3d}$$

$$\mu_2(0) = \mu_1(t_{\text{f}}) \qquad \mu_3(0) = \mu_2(t_{\text{f}}) \qquad \mu_1(0) = \mu_3(t_{\text{f}}). \tag{6.3e}$$

Optimal Trade-offs Between Copper Loss and Torque Ripple

In the literature only control corresponding to two extreme control objectives have been investigated, either to maximize the efficiency or to minimize the torque ripple. The results in this section illustrates how trade-offs between the two objectives can be made. Three operating conditions were examined, high speed and low load (100 rad/s and 4 Nm), high speed and high load (100 rad/s and 15 Nm) and finally low speed and high load(20 rad/s and 20 Nm).

Resulting copper losses and torque-ripple for the different experiments are listed in tables 6.1, 6.2 and 6.3. The results are also visualized in figures 6.1, 6.8 and 6.10 respectively.

Control Type	TR_{abs}	TR_{rms}	Copper Loss [w]
On/Off Control	**2.039**	**1.525**	**32.463**
Optimal, $\alpha_{smooth} = 0$	**1.625**	**1.222**	**31.477**
Optimal, $\alpha_{smooth} = 0.5$	1.436	1.041	31.887
Optimal, $\alpha_{smooth} = 1$	1.122	0.792	33.208
Optimal, $\alpha_{smooth} = 2$	**0.789**	**0.528**	**35.134**
Optimal, $\alpha_{smooth} = 3.5$	0.562	0.357	36.698
Optimal, $\alpha_{smooth} = 5$	0.444	0.272	37.579
Optimal, $\alpha_{smooth} = 15$	**0.216**	**0.116**	**39.498**
Optimal, $\alpha_{smooth} = 50$	0.099	0.056	40.535
Optimal, $\alpha_{smooth} = 100$	0.064	0.047	40.836
Optimal, $\alpha_{smooth} = 200$	0.045	0.043	41.088
Optimal, $\alpha_{smooth} = 400$	0.030	0.040	41.371
Optimal, $\alpha_{smooth} = 1000$	**0.021**	**0.039**	**41.634**
DITC	**0.051**	**0.025**	**43.555**

Table 6.1: The copper losses and torque ripple at $\omega = 100\,\text{rad/s}$ and $\tau_{load} = 4\,\text{Nm}$ for different control approaches.

High Speed and Low Torque Experiments were made with a velocity of $\omega = 100\,\text{rad/s}$ and a torque demand of $\tau_{load} = 4\,\text{Nm}$.

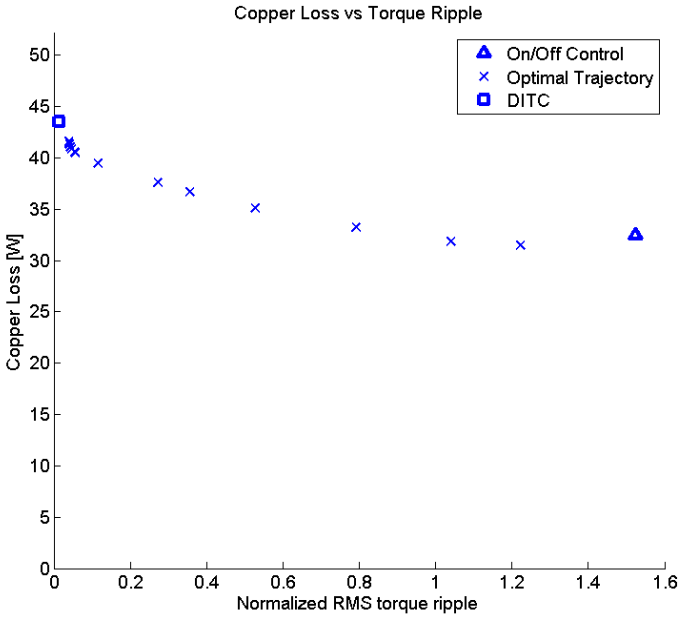

Figure 6.1: Copper loss plotted as a function of torque ripple for the results in table 6.1.

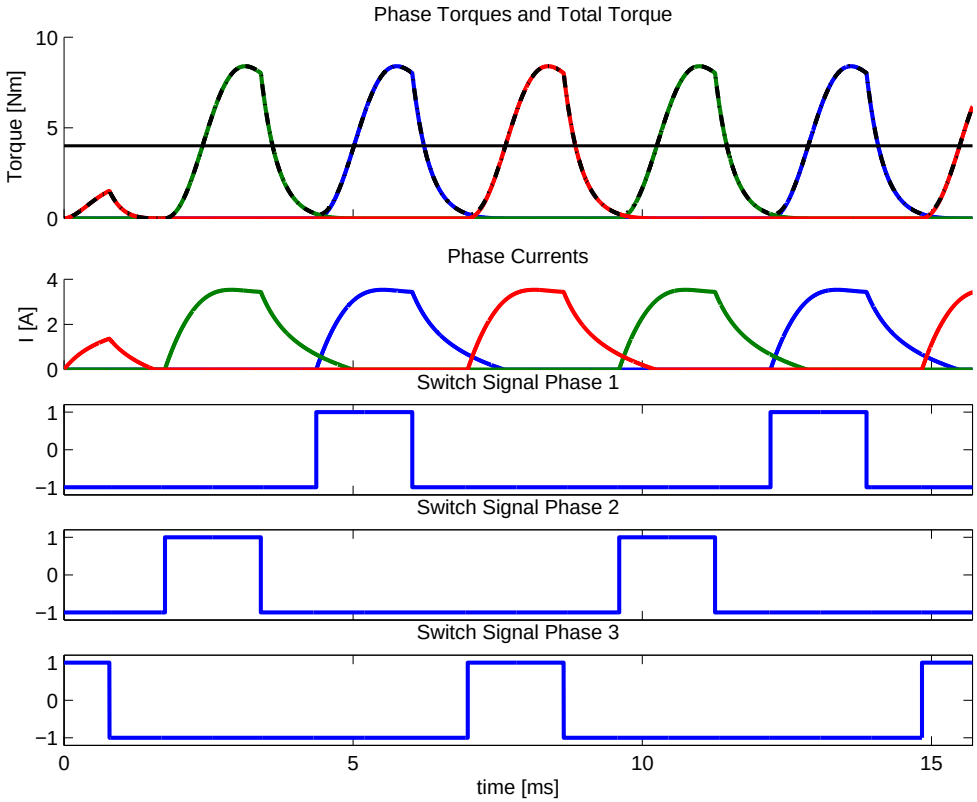

Figure 6.2: Waveforms corresponding to line 1 in table 6.1 (On/Off Control).

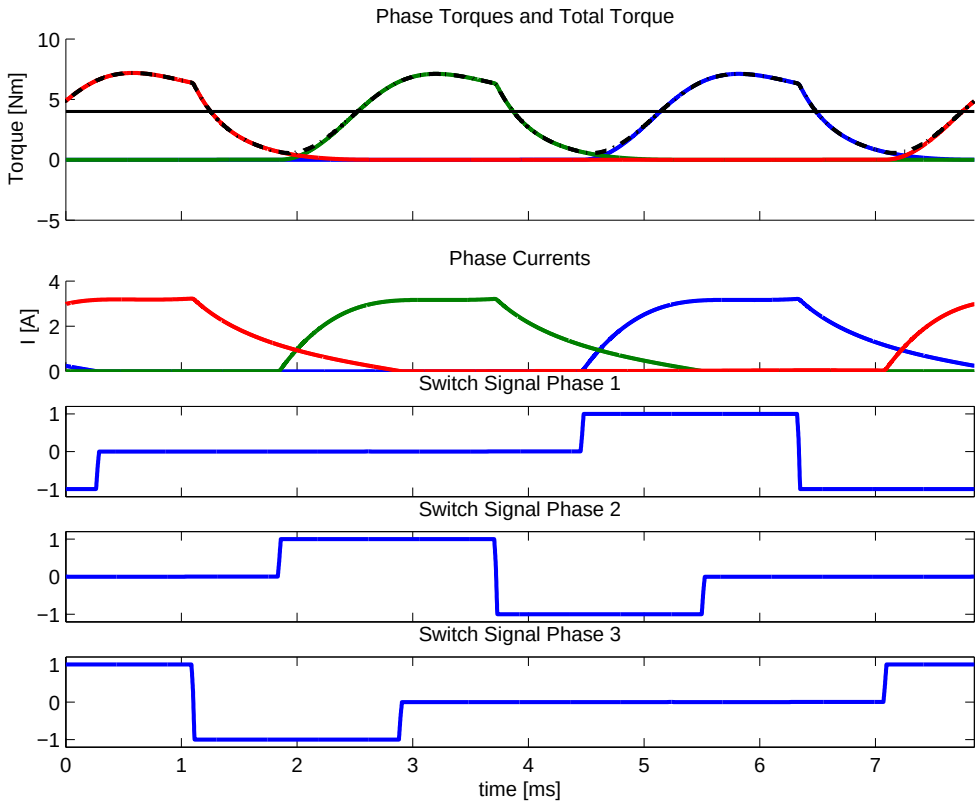

Figure 6.3: Waveforms corresponding to line 2 in table 6.1 ($\alpha_{\text{smooth}} = 0$).

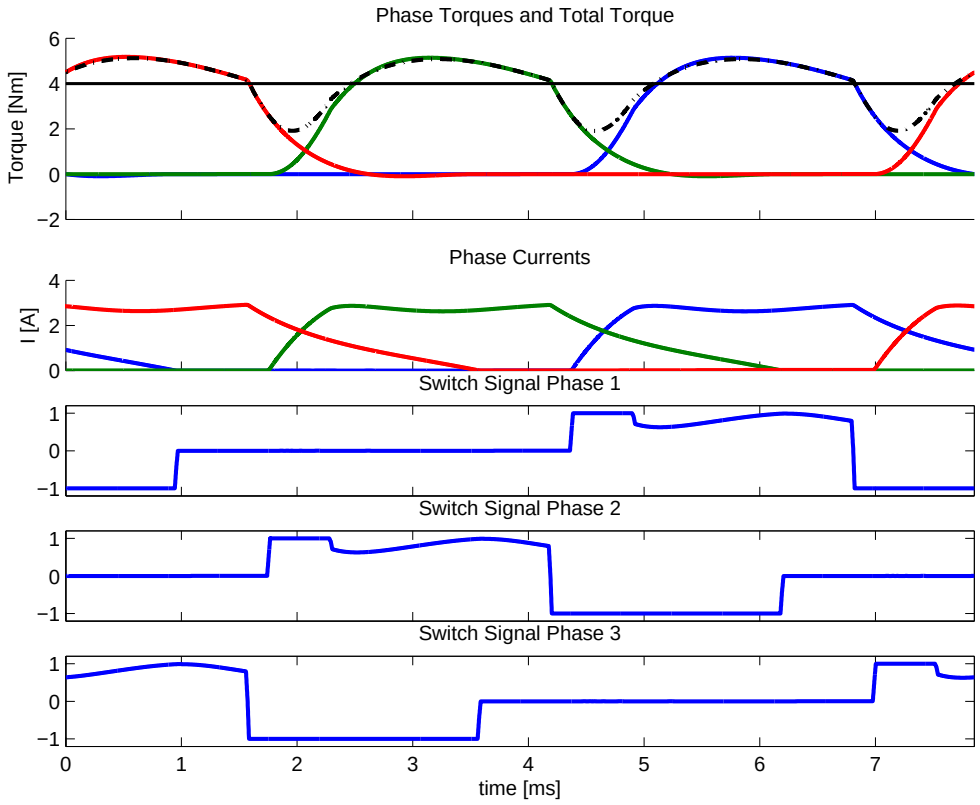

Figure 6.4: Waveforms corresponding to line 5 in table 6.1 ($\alpha_{\text{smooth}} = 2$).

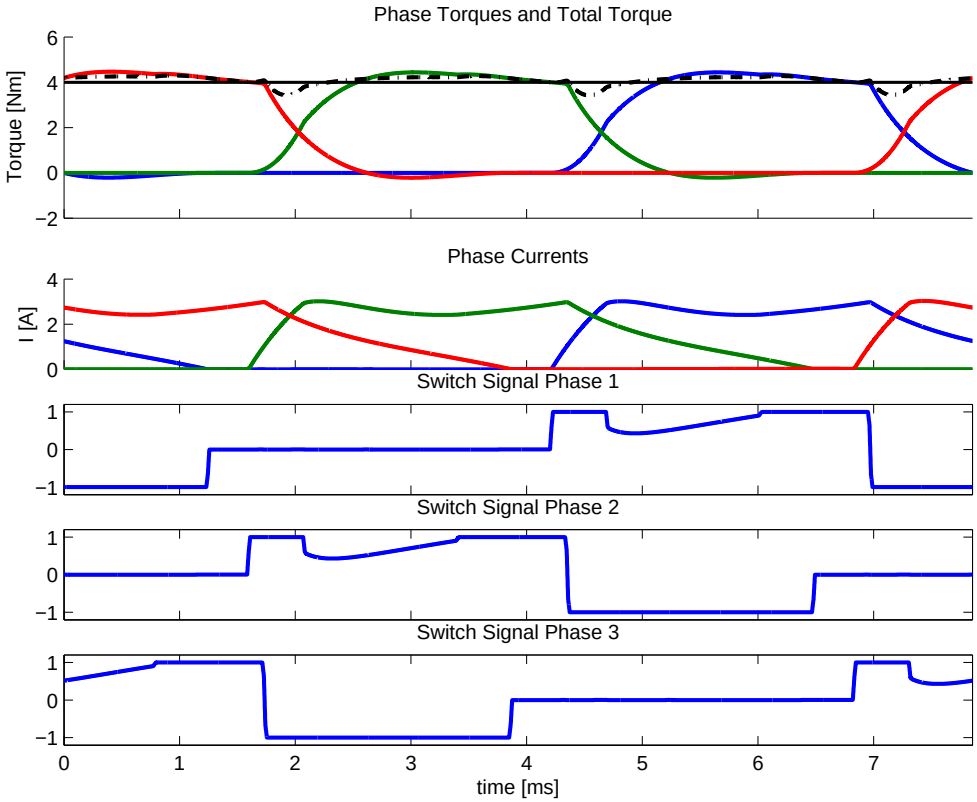

Figure 6.5: Waveforms corresponding to line 8 in table 6.1 ($\alpha_{\text{smooth}} = 15$).

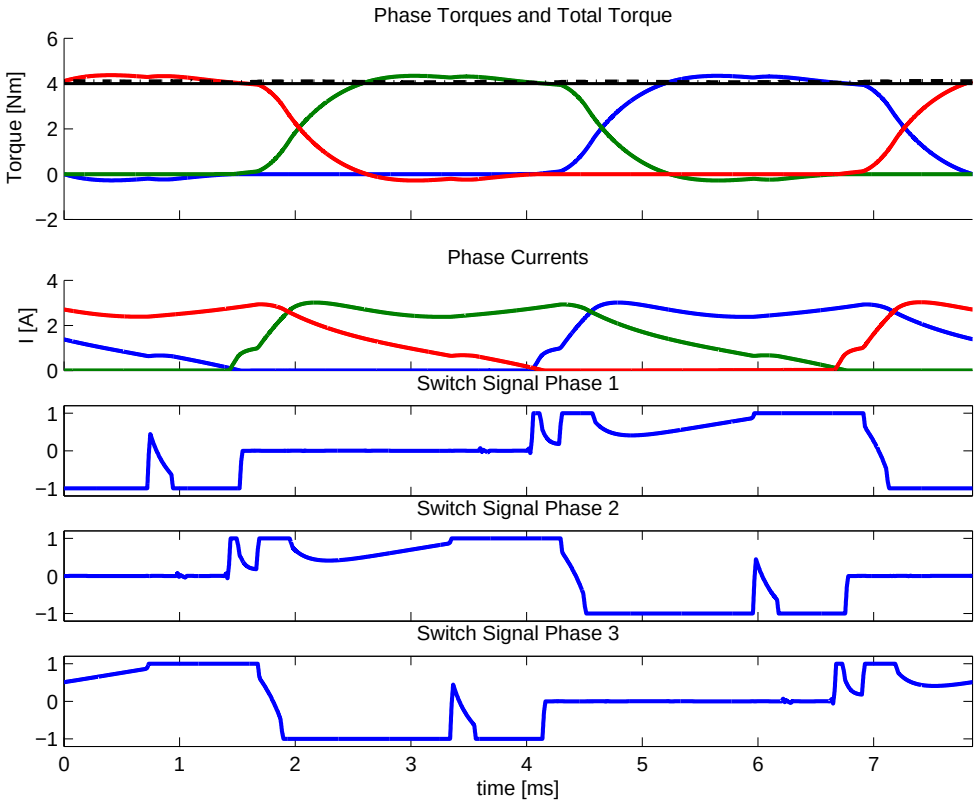

Figure 6.6: Waveforms corresponding to line 13 in table 6.1 ($\alpha_{\text{smooth}} = 1000$).

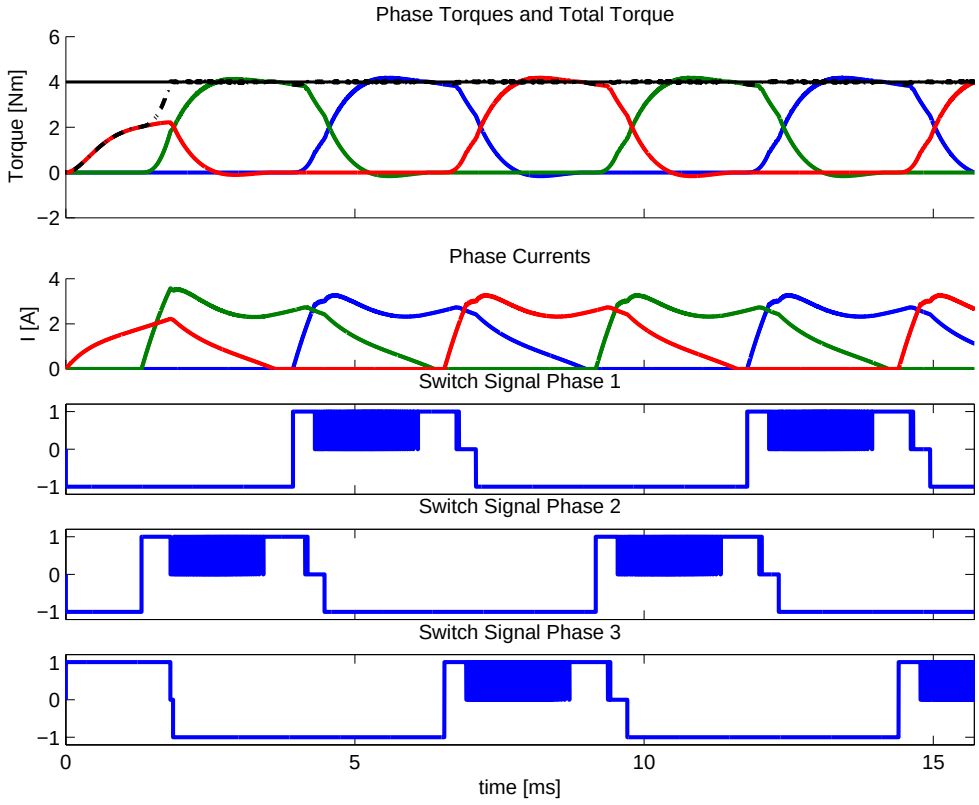

Figure 6.7: Waveforms corresponding to line 14 in table 6.1 (DITC).

High Speed and High Torque Experiments were made at $\omega = 100\,\text{rad/s}$ and with a torque demand of $\tau_{\text{load}} = 15\,\text{Nm}$.

Note in figure 6.9 how the phase currents never goes to zero although negative torque is produced. This happens because it is the only way to reduce the torque ripple even if it is very bad in terms of efficiency.

Control Type	TR_{abs}	TR_{rms}	Copper Loss [W]
On/Off Control	0.975	1.277	190.768
Optimal, $\alpha_{\text{smooth}} = 0$	0.958	1.241	191.022
Optimal, $\alpha_{\text{smooth}} = 1$	0.755	0.965	194.409
Optimal, $\alpha_{\text{smooth}} = 2$	0.683	0.890	197.495
Optimal, $\alpha_{\text{smooth}} = 3$	0.573	0.786	205.788
Optimal, $\alpha_{\text{smooth}} = 8$	0.446	0.612	227.358
Optimal, $\alpha_{\text{smooth}} = 16$	0.353	0.445	257.412
Optimal, $\alpha_{\text{smooth}} = 40$	0.229	0.259	306.781
Optimal, $\alpha_{\text{smooth}} = 100$	**0.146**	**0.144**	**350.677**
Optimal, $\alpha_{\text{smooth}} = 200$	0.094	0.081	385.015
Optimal, $\alpha_{\text{smooth}} = 500$	0.069	0.057	404.246

Table 6.2: The copper losses and torque ripple for different control approaches with $\omega = 100\,\text{rad/s}$, $\tau_{\text{load}} = 15\,\text{Nm}$

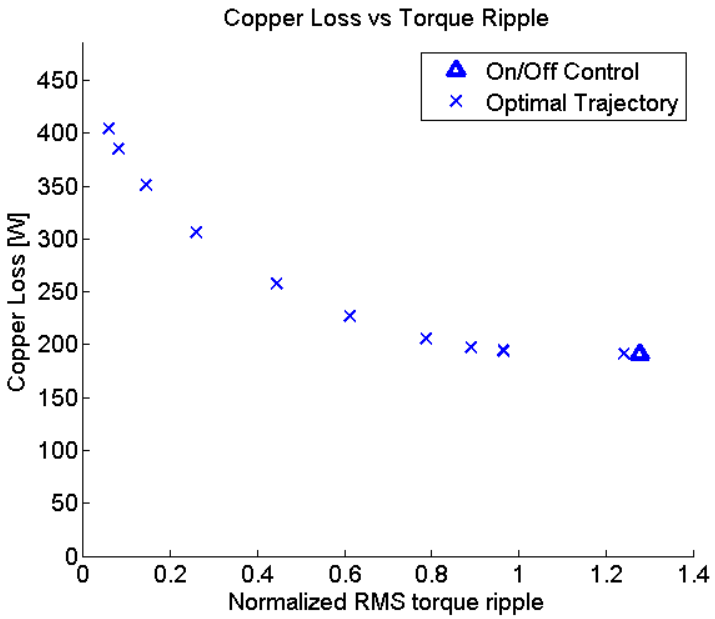

Figure 6.8: Copper loss plotted as a function of torque ripple for the results in table 6.2.

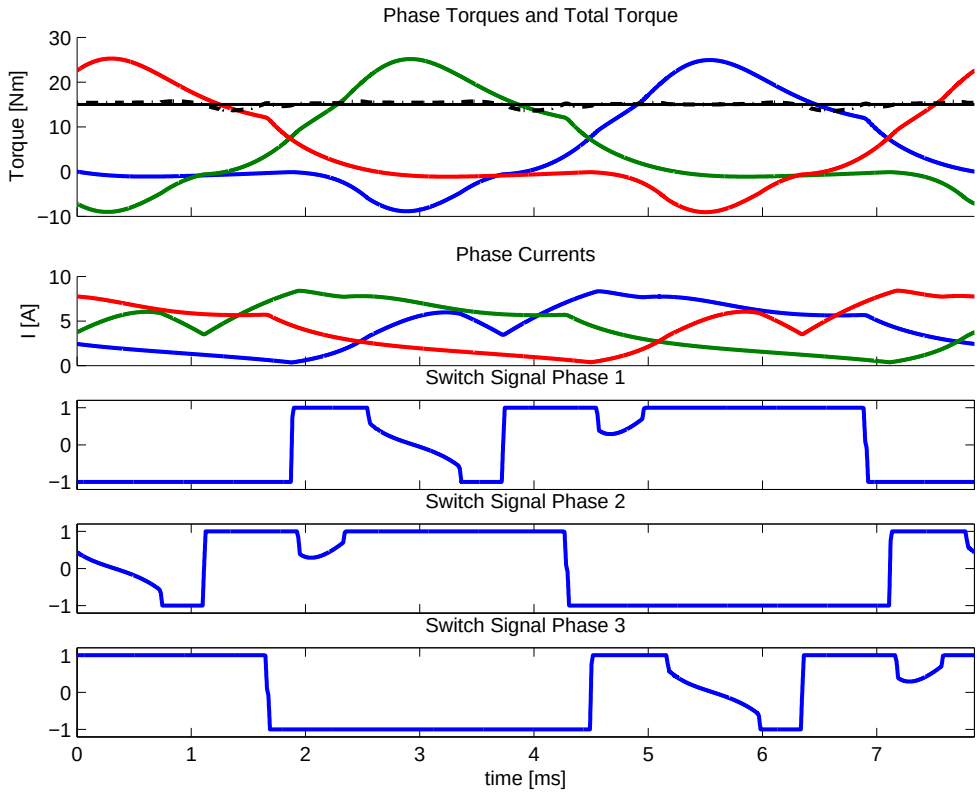

Figure 6.9: Typical phase trajectories at a high load torque when torque ripple is penalized. Note how the currents never goes to zero even though negative torque is produced.

Low Speed and High Torque Experiments were made at $\omega = 20\,\text{rad/s}$ and with a torque demand of $\tau_{\text{load}} = 20\,\text{Nm}$. Note that the efficiency at the high torque demand of 20 Nm is pretty poor considering that only 400 W is converted to mechanical energy. Considering only copper losses, this gives an efficiency of between 60% and 64%.

Discussion It has been seen by comparing the performance of the optimal trajectories to the conventional control approaches that they indeed give lower torque-ripple than On/Off control but higher efficiency than DITC. In figures 6.1 through 6.7 it is seen how the optimal trajectories provide a smooth transition between On/Off control and DITC. In figure 6.1 it is how the performance of the generated optimal trajectories line out a pareto-optimal front in the efficiency/torque-ripple diagram.

Note also in the same figure that the point corresponding to On/Off control is behind the pareto-optimal front, i.e. the conventional On/Off control is not optimal with respect to efficiency (however the switching losses in the converter has not been modeled).

It should be pointed out that there are no guarantees that the optimal trajectories in this or the following sections actually are globally optimal since the differential equations in (5.22) are nonconvex. However from the comparisons in figures 6.1, 6.8 and 6.10 it is seen that at least the optimal trajectories performs no worse than the conventional control approaches. This means that even if they are not optimal they are at least useful.

Control Type	TR_{abs}	TR_{rms}	Copper Loss [W]
Optimal, $\alpha_{smooth} = 0$	1.833	2.750	225.324
Optimal, $\alpha_{smooth} = 0.2$	1.059	1.548	232.627
Optimal, $\alpha_{smooth} = 0.5$	0.650	0.939	242.103
Optimal, $\alpha_{smooth} = 1$	0.396	0.568	249.876
Optimal, $\alpha_{smooth} = 2$	0.221	0.315	256.050
Optimal, $\alpha_{smooth} = 3$	0.152	0.217	258.664
Optimal, $\alpha_{smooth} = 5$	0.093	0.132	261.017
Optimal, $\alpha_{smooth} = 10$	0.046	0.064	262.962
Optimal, $\alpha_{smooth} = 25$	0.018	0.025	264.212
Optimal, $\alpha_{smooth} = 100$	0.011	0.015	264.863
DITC	0.006	0.005	266.103

Table 6.3: Copper losses and torque ripple for different control approaches at a speed of $\omega = 20\,\text{rad/s}$ and a torque demand of $\tau_{load} = 20\,\text{Nm}$.

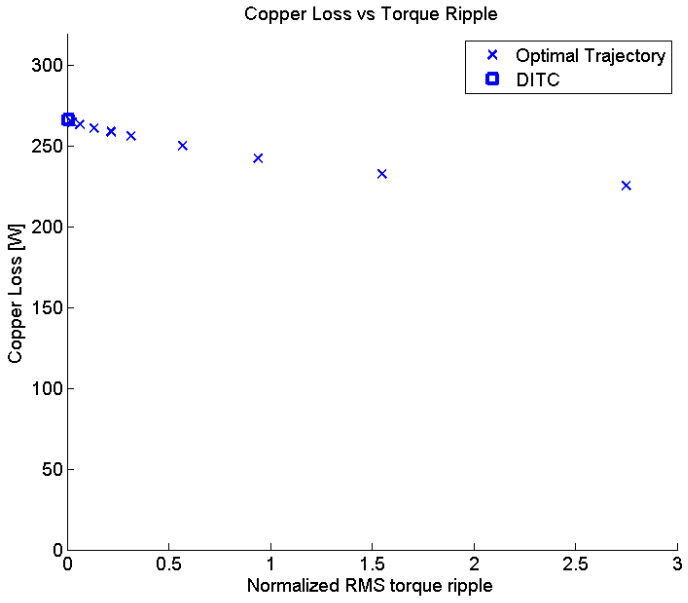

Figure 6.10: Copper loss plotted as a function of torque ripple for the results in table 6.3.

Influence of Current Limits

In On/Off control the current is permitted to rise to a certain current limit where it is kept constant until it is turned off. Also direct instantaneous torque controllers have limits on the currents in order to prevent the motor from overheating. As was remarked in section 5.6, when computing optimal phase trajectories over some given time interval, there is no need for instantaneous limits on the currents but rather on the average losses over a time interval corresponding to the thermal time constants of the inverter and SRM.

Optimal trajectories subject to different current limits were computed for a

speed of 30 rad/s and a high torque demand of 25 Nm. The results are shown in table 6.4. The waveforms for the optimal trajectory without current constraints are shown in figures 6.11 and those for a current limit of 9 A in 6.12.

Current Limit [A]	TR_{abs}	TR_{rms}	Copper Loss [W]
No Limit	**1.688**	**2.827**	**309.647**
10.0	1.528	2.660	310.023
9.0	**1.199**	**1.990**	**314.972**
8.0	0.451	0.751	349.262

Table 6.4: Results of simulations made to illustrate the negative impact of current limits on efficiency.

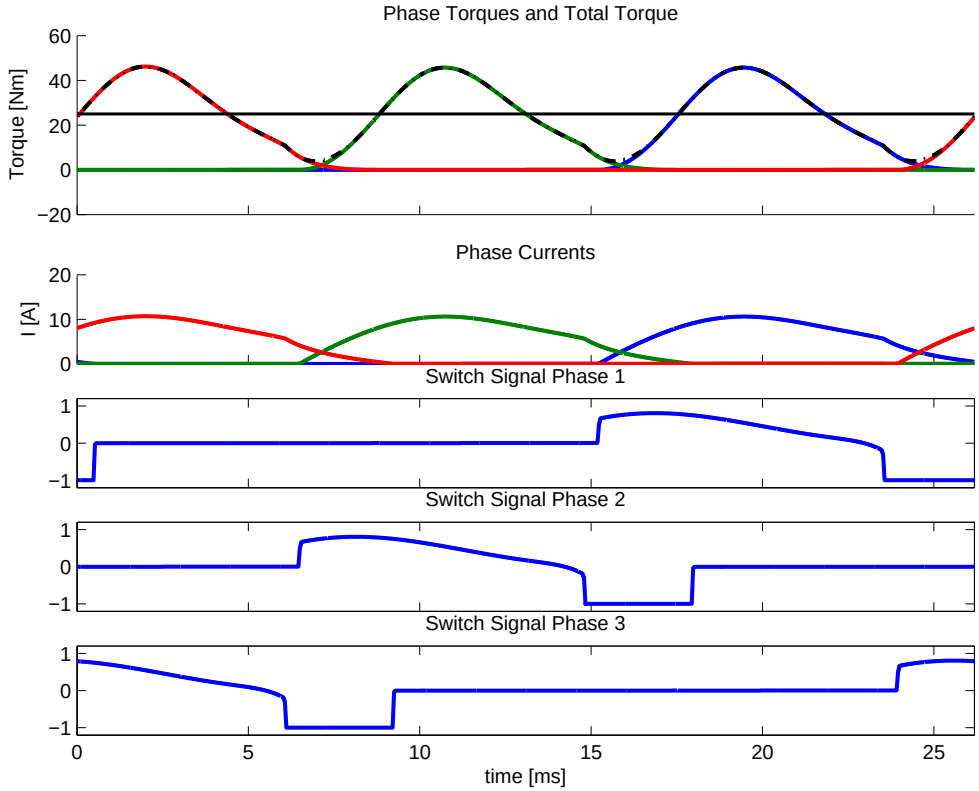

Figure 6.11: Waveforms corresponding to line 1 in table 6.4 (no current limit).

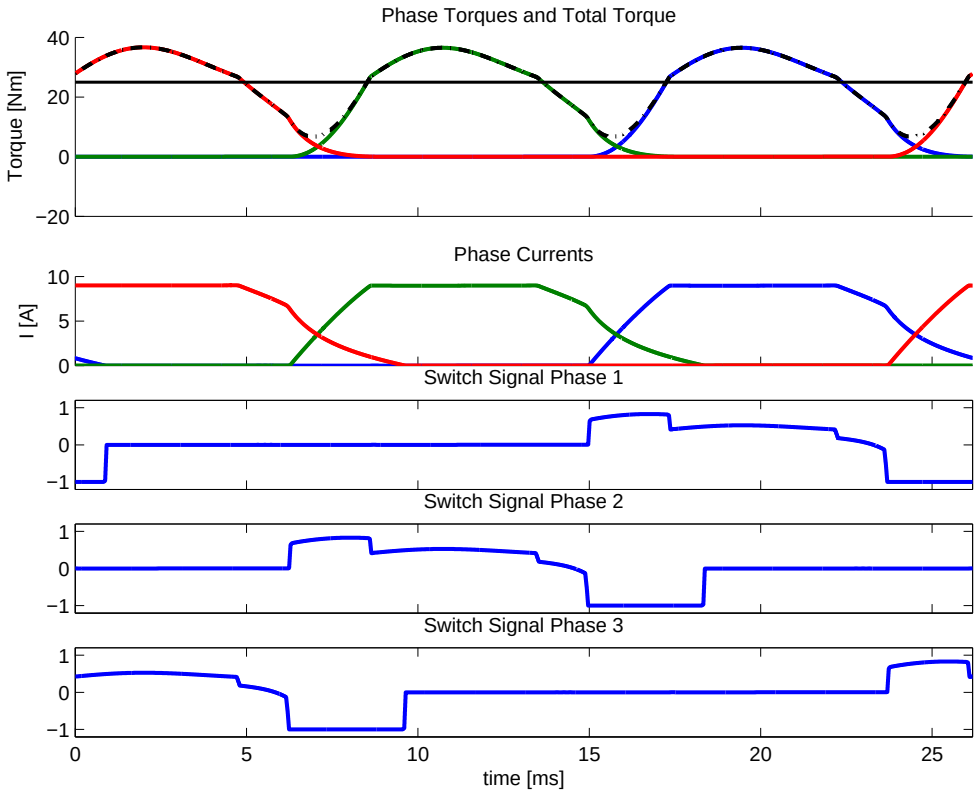

Figure 6.12: Waveforms corresponding to line 3 in table 6.1 ($I_{\max} = 9\,\mathrm{A}$).

Discussion From the results in table 6.4 it is seen that the optimal performance without current limits is significantly higher than when currents constraints are imposed. This is natural considering that the optimal value in an optimization problem typically improves if active constraints are removed.

In practice it might not desirable to remove the current limits since these provide a reliable way of preventing the motor from overheating.

Influence of Iron Losses in the Objective Function

Most control approaches for SRMs only try to minimize the copper losses since they are the most important loss mechanism and by far the easiest to model. In section 5.2 expressions for the iron losses were derived and although qualitative in nature, it should be possible to lower the losses by taking them into account when controlling the motor.

Comparisons of the performance of different trajectories were made for $\omega = 100\,\mathrm{rad/s}$ and $\tau_{\mathrm{load}} = 8\,\mathrm{Nm}$. Results are shown in table 6.5.

To investigate the impact of taking the iron losses into account for a motor with relatively higher iron losses the same experiment was done using 4 times larger iron loss coefficients. The results are shown in table 6.6.

A comparison between phase trajectories optimized with respect to just copper losses and with respect to iron losses as well are shown in figure 6.13.

Discussion

From table 6.5 it is seen that the total losses may be lowered by 2-3% by taking all the losses into account when controlling of the motor. If the iron losses were greater, then the energy savings would also be correspondingly greater, from

TR_{abs}	TR_{rms}	Copper Loss [W]	Hysteresis Loss [W]	Eddy Current Loss [W]	Switching Loss [W]	Total Loss [W]
0.53	1.43	78.522	6.669	10.402	3.909	99.519
0.47	1.38	76.860	7.484	12.361	4.016	100.736
0.46	1.29	77.710	6.968	11.088	3.943	99.725
0.41	1.26	76.661	7.852	13.278	4.075	101.881
0.53	1.41	78.522	6.669	10.402	3.909	99.519
0.46	1.35	76.919	7.426	12.217	4.007	100.585
0.47	1.32	77.785	6.927	11.010	3.939	99.678
0.38	1.21	76.657	7.946	13.516	4.091	102.225

Table 6.5: Losses for optimal trajectories computed with respect to objective functions comprising different loss terms (underlined).

TR_{abs}	TR_{rms}	Copper Loss [W]	Hysteresis Loss [W]	Eddy Current Loss [W]	Switching Loss [W]	Total Loss [W]
0.70	**1.90**	**87.324**	**21.645**	**30.180**	**3.841**	**143.005**
0.57	1.50	79.130	26.007	40.053	3.892	149.098
0.65	1.73	83.675	22.958	33.209	3.845	143.704
0.38	1.22	76.661	31.407	53.111	4.075	165.269
0.78	2.12	87.324	21.646	30.180	3.841	143.006
0.55	1.49	79.130	26.007	40.053	3.892	149.098
0.62	1.64	83.675	22.955	33.210	3.845	143.701
0.46	**1.33**	**76.657**	**31.785**	**54.063**	**4.091**	**166.611**

Table 6.6: Losses for optimal trajectories computed with respect to objective functions comprising different loss terms (underlined). The iron losses in the motor were taken to be 4 times larger than for the results in table 6.5

table 6.6 where the iron losses were four times larger the losses were reduced by more than 13 %.

Including the converter losses in the objective function had little effect on the optimal trajectories (although it is important to minimize the switching losses through a good switching scheme [18, 20]).

Naturally a good model for the iron losses is required in order to take them into account when designing the control law, since they are intrinsically hard to model it is practically challenging to take them into account. The results in this sections still high lights how much could be gained by using a more sophisticated controller.

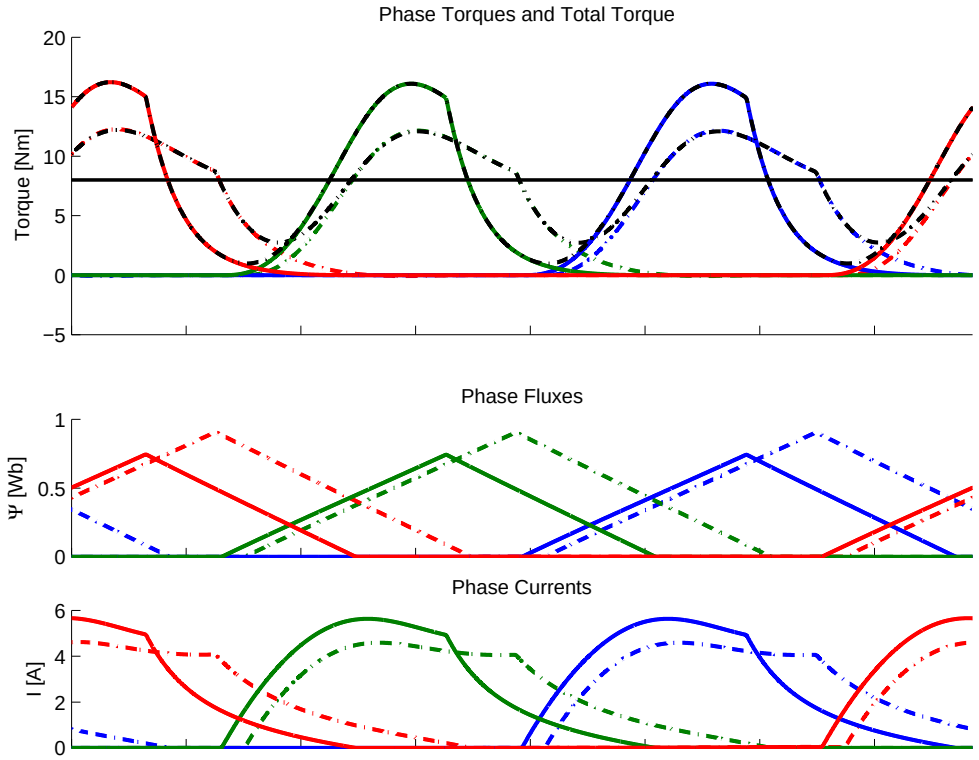

Figure 6.13: Comparison of torque profiles, phase flux linkage profiles and current profiles optimized with respect to just copper losses (dash dotted line) and a complete loss model (solid line). The two cases correspond to the first and last lines of table 6.6.

6.3 Test Case 2: Point-to-point Movement

In motion control applications such as robotics, the electric motors are typically required to make a rotation between two angular positions. In this section efficiency improvements of using the optimal trajectories for this type of movement are considered.

The conventional approach could be considered to first generate a total torque trajectory based on a quadratic penalty on the torque $(\tau_{\text{el}})^2$ and then optimally allocate the phase torques in order to minimize the copper losses. This design approach would more or less correspond to the following objective function

$$J = \int_0^{t_{\text{f}}} \sum_{k=1}^{3} R i_k^2 + \alpha(\tau_{\text{el}})^2 \, dt, \tag{6.4}$$

If the α is large it means that minimizing $(\tau_{\text{el}})^2$ would be considered to be the primary objective and then minimizing the copper losses to be less important.

Optimal trajectories based on the complete model (5.22) and the modified cost function (6.4) were computed for a third of a revolution (i.e. $2\pi/3$radians) point-to-point movements. The initial and final angular velocities were required to be zero.

The optimal trajectory based on the simplified cost function is shown in figure 6.15 and the optimal trajectory for the true cost function is shown in figure 6.14. A comparison of the energy losses in the two different cases is given

in 6.7.

	Copper Loss [J]
Optimal Trajectory	**11.737**
T^2-Optimal Trajectory	**17.175**

Table 6.7: Comparison of copper losses for trajectories optimized with respect to a complete loss model and a quadratic penalty on the total torque.

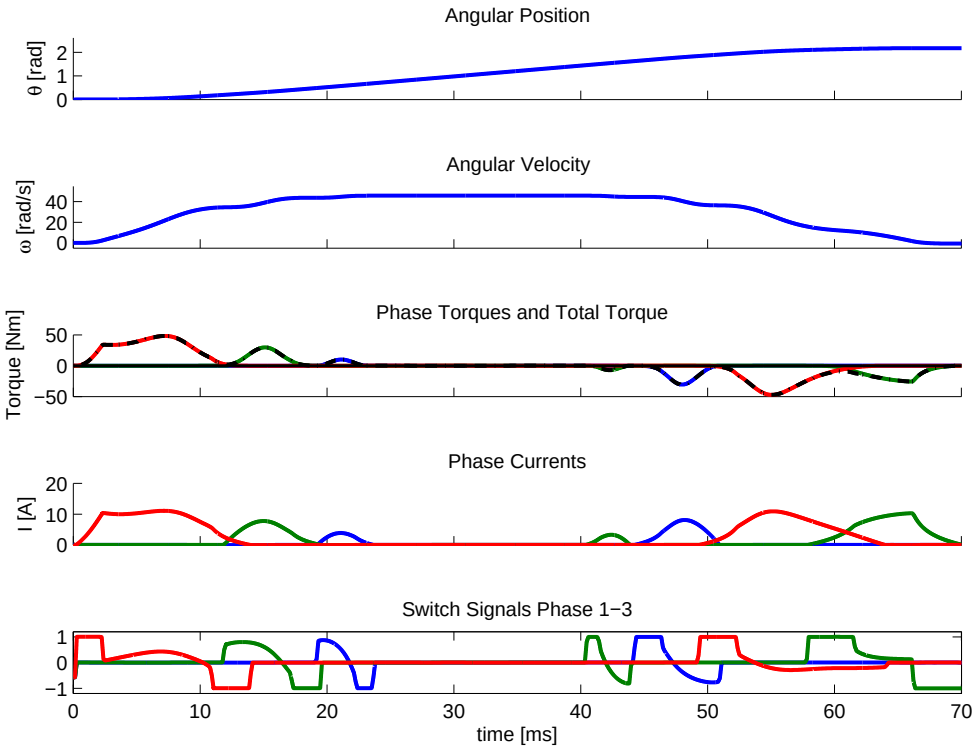

Figure 6.14: Trajectories optimized with respect to a complete loss model.

Discussion

It is seen in table 6.7 that there are significant energy savings to be made by using the optimal trajectories based on the complete model. However comparing figures 6.14 it should be noted that the torque fluctuations for this type of trajectory are much more severe than for the simplified model.

Although it seems unlikely that the optimally computed trajectories would be useful in practice, given their long computation time, they indicate that the naïve approach is far from optimal. Also it was surprising (at least to the author) that JModelica and IPOPT were able to handle the large optimal control problem given its size and nonlinear dynamics.

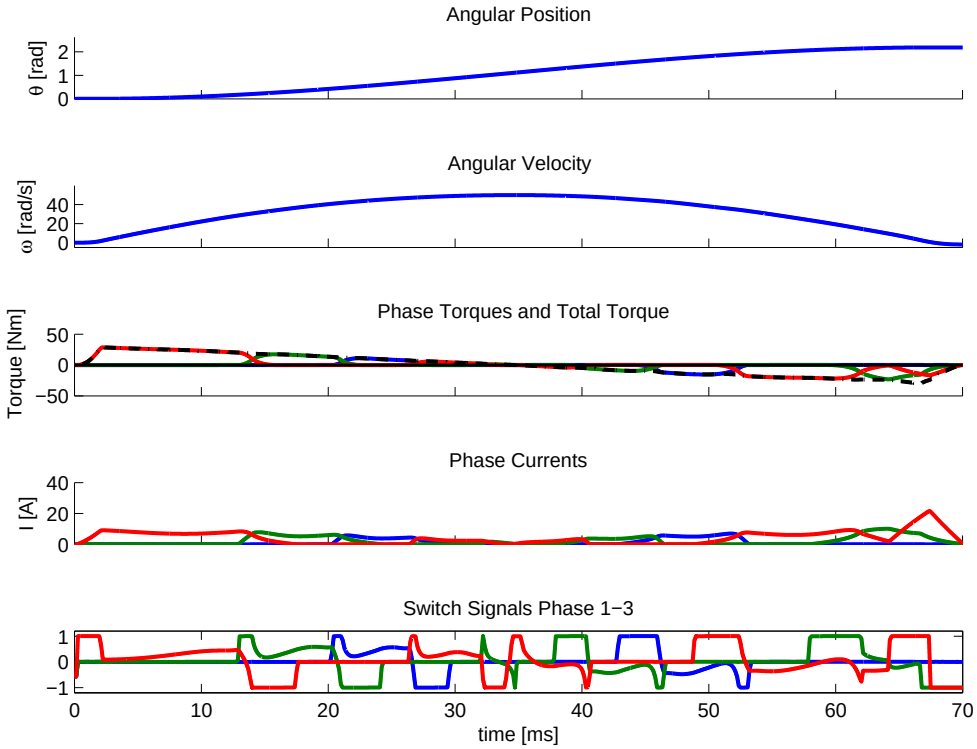

Figure 6.15: Trajectories optimized with respect to a quadratic penalty on the total torque.

7. Problem Structure

Considering the problem of optimally allocating the torque between the different phases in constant velocity operation, it is of interest to note that the problem seems to be convex if the control variables are chosen to be the phase torques themselves and only copper losses are included in the objective function. Choosing the phase torques as the states is no different from using the phase currents or phase fluxes since the phase torque is a monotonically increasing function of the phase current. The choice of the phase torques as states is motivated by that the equality constraint 7.2 becomes convex. Also it has to be assumed that the inertia of the load is large enough that the velocity remains constant, $\omega(t) = \omega_0$.

Formulating the optimal control problem with the phase torques τ_k as control variables and the angle given by $\theta = \omega_0 t$, gives the following minimization problem,

$$\text{minimize} \qquad \int_0^{t_\text{f}} \sum_{k=1}^{3} R i_k(\theta, \tau_k)^2 \, dt, \tag{7.1}$$

subject to the following equality constraint

$$\tau_1 + \tau_2 + \tau_3 = \tau_\text{ref}(\theta), \tag{7.2}$$

the following inequality constraints

$$i_k(\theta, \tau_k) \leq i_\text{max} \qquad k = 1, 2, 3 \tag{7.3}$$

$$g_k(\theta, \tau_k) \leq \dot{\tau} \leq h_k(\theta, \tau_k) \qquad k = 1, 2, 3, \tag{7.4}$$

and some suitable boundary conditions. The functions $g_k(\theta, \tau_k)$ and $h_k(\theta, \tau_k)$ give the maximal rate of change for the torque at a given state of the motor.

In the above inequality g_k and h_k are determined from the voltage constraints $-V_\text{dc} \leq \frac{d\psi_k}{dt} - R i_k \leq V_\text{dc}$. The right bound in 7.4 can be written

$$\dot{\tau}_k \leq h_k(\theta, \tau_k) = \frac{\partial \tau_k}{\partial \psi_k}(\theta, \tau_k)(V_\text{dc} - R i_k(\theta, \tau_k)) + \frac{\partial \tau_k}{\partial \theta}(\theta, \tau_k)\omega.$$

In figure 7.1 it is seen that $\partial \tau_k / \partial \psi_k$ is concave as a function of τ_k and $\partial \tau_k / \partial \theta$ is linear (which may be realized by the form of the expression used for the torque $\tau_k = g(i)f(\theta)$). This implies that if the term $\frac{\partial \tau_k}{\partial \psi_k} R i_k(\theta, \tau_k)$ is negligible, then the constraints are convex regardless of the velocity ω.

The product $\frac{\partial \tau_k}{\partial \psi_k} i_k(\theta, \tau_k)$ is not convex, but since $R i_k(\theta, \tau_k)$ is small compared to V_dc, the effects of the nonconvex term should be be limited.

Even though $i_k(\theta, \tau_k)$ is not convex, squaring it makes it so, which is seen in figure 7.2, thus the objective function is convex.

Also the constraint s $i_k(\theta, \tau_k) \leq i_\text{max}$ give rise to a convex feasible set since $i_k(\theta, \tau_k)$ is a monotonically increasing (decreasing) function of τ_k when $\tau_k \geq 0$ ($\tau_k \leq 0$).

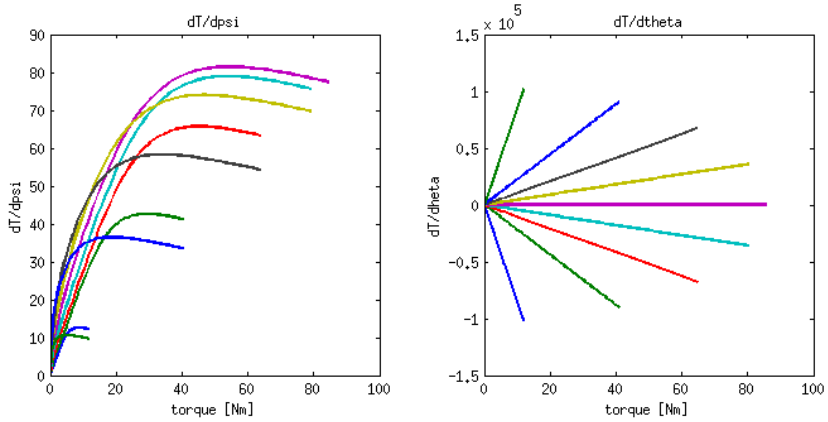

Figure 7.1: Partial derivatives of the torque τ_k with respect to ψ_k and θ.

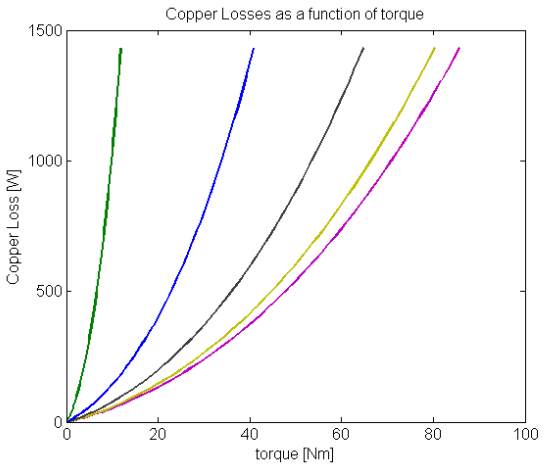

Figure 7.2: The copper losses as a function of the torque for different angles θ.

8. Conclusion

8.1 Pros and cons of using optimally designed phase trajectories

The first part of the thesis discussed whether a switched reluctance motor would be able to compete with a permanent magnet motor. Although the answer is very much application dependent, the many recent advances in the mechanical design of SRMs mentioned in chapter 4 indicate that today's SRMs are far from their full potential. Even so the SRM will necessarily be somewhat less efficient than the corresponding permanent magnet motors and to obtain the same torque output the SRM would have to be slightly bigger. If these downsides are outweighed by a more robust design and a significantly lower price, then yes, the SRM would indeed be able to compete with permanent magnet motors.

The second part of this thesis looked at how trade-offs in SRM performance can be made through the control design. Formulating and solving an optimal control problem made it possible to make trade-offs that are not possible with conventional control approaches. It was also possible to include the dynamic iron losses into the optimziation problem. However the amount of computations required and the complexity of implementation makes the approach impractical for real-world applications.

A perhaps better way of looking at the results in the second half of the thesis is that they give an indication of the best possible performance that can be achieved by making trade-offs in control design. This gives an upper bound for the performance of simplified but more practically feasible controllers.

An interesting feature is that the weights in the cost function may be updated as the operating conditions change. For example by adjusting the α_{smooth} it is possible to put more or less emphasis on keeping the torque ripple low. Thus in for example an electric vehicle application it would be possible to emphasize high efficiency when battery charge is low and to emphasize smooth torque when there are picky passengers in the car.

The use of the Modelica language made it very convenient to model the electromechanics of the SRM. Previously made approaches to modeling and simulation of SRMs, for example [2], seem cluttered in comparison. The optimal trajectories computed by JModelica achieve good performance compared to conventional control approaches, but there are no guarantees that they are globally optimal.

9. Outlook and Future Work

There are several further things that it would be possible to study using the context of the formulated optimal control problem.

It should be possible model more of the power electronics, for example the DC link capacitance. Often it is desirable to keep its charge within certain limits and to avoid current ripple in order prolong its lifetime. This should be relatively easy to do by introducing an additional state for the capacitor charge in the model.

Also it would be interesting to investigate if there are any gains in using a more advanced converter structures with more degrees of freedom, for example soft-switching converters.

Although the motoring mode for an SRM is relatively straightforward, it is more complex to control it as a generator. This is because the charge in the DC-link/capacitor must first be used to energize a phase before the phase can be de-energized in order to recover electric energy from the kinetic energy of the load. There are also problems with instability in this mode, so there could be significant gains in doing it in an optimal fashion.

Although almost always neglected, there are cross couplings between the phases to some extent. This effect could also quite easy be included in the optimal control problem.

Finally, as mentioned in the first chapter, the implemented trajectory optimization scheme could be made to fit nicely in co-design process.

A. Bibliography

[1] "Sr drives." `http://www.srdrives.com/washing-machine.shtml`. Accessed: 2012-07-20.

[2] R. De Doncker, D. Pulle, and A. Veltman, *Advanced Electrical Drives: Analysis, Modeling, Control*. Springer Verlag, 2011.

[3] M. T. L. Jin-Woo Ahn, *Torque Control*, ch. 8. Switched Reluctance Motor. InTech, 2011. Available from: http://www.intechopen.com/books/torque-control/switched-reluctance-motor.

[4] B. Mecrow, J. Finch, E. El-Kharashi, and A. Jack, "Switched reluctance motors with segmental rotors," *Electric Power Applications, IEE Proceedings* -, vol. 149, pp. 245 – 254, july 2002.

[5] R. Vandana, N. Vattikuti, and B. Fernandes, "A novel high power density segmented switched reluctance machine," in *Industry Applications Society Annual Meeting, 2008. IAS '08. IEEE*, pp. 1 –7, oct. 2008.

[6] R. Madhavan and B. Fernandes, "A novel axial flux segmented srm for electric vehicle application," in *Electrical Machines (ICEM), 2010 XIX International Conference on*, pp. 1 –6, sept. 2010.

[7] C. Lee and R. Krishnan, "New designs of a two-phase e-core switched reluctance machine by optimizing the magnetic structure for a specific application: Concept, design, and analysis," *Industry Applications, IEEE Transactions on*, vol. 45, pp. 1804 –1814, sept.-oct. 2009.

[8] M. Abbasian, M. Moallem, and B. Fahimi, "Double-stator switched reluctance machines (dssrm): Fundamentals and magnetic force analysis," *Energy Conversion, IEEE Transactions on*, vol. 25, pp. 589 –597, sept. 2010.

[9] C. S. Kim, G. Lee, K. Lee, J. Lee, Y. Cho, J. H. Won, H. Shin, C. Choi, and H. K. Bae, "Design of π-core and π^2-core pm-aided switched reluctance motors," in *Electric Vehicle Conference (IEVC), 2012 IEEE International*, pp. 1 –6, march 2012.

[10] F. Daldaban and N. Ustkoyuncu, "New disc type switched reluctance motor for high torque density," *Energy conversion and management*, vol. 48, no. 8, pp. 2424–2431, 2007.

[11] T. J. E. Miller, *Electronic Control of Switched Reluctance Machines*. Newnes, 2001.

[12] T. Celik, *Segmental rotor switched reluctance drives*. PhD thesis, Newcastle University upon Tyne, 2011.

[13] J. Reinert, R. Inderka, M. Menne, and R. De Doncker, "Optimizing performance in switched-reluctance drives," *Industry Applications Magazine, IEEE*, vol. 6, pp. 63 –70, jul/aug 2000.

[14] B. Mecrow, E. El-Kharashi, J. Finch, and A. Jack, "Preliminary performance evaluation of switched reluctance motors with segmental rotors," *Energy Conversion, IEEE Transactions on*, vol. 19, pp. 679 – 686, dec. 2004.

[15] R. Krishnan, *Switched reluctance motor drives: modeling, simulation, analysis, design, and applications*. CRC, 2001.

[16] N. Fuengwarodsakul, M. Menne, R. Inderka, and R. De Doncker, "High-dynamic four-quadrant switched reluctance drive based on ditc," *Industry Applications, IEEE Transactions on*, vol. 41, pp. 1232 – 1242, sept.-oct. 2005.

[17] I. Husain, "Minimization of torque ripple in srm drives," *Industrial Electronics, IEEE Transactions on*, vol. 49, pp. 28 –39, feb 2002.

[18] R. Inderka and R. De Doncker, "Ditc-direct instantaneous torque control of switched reluctance drives," *Industry Applications, IEEE Transactions on*, vol. 39, pp. 1046 – 1051, july-aug. 2003.

[19] H. Brauer, M. Hennen, and R. De Doncker, "Control for polyphase switched reluctance machines to minimize torque ripple and decrease ohmic machine losses," *Power Electronics, IEEE Transactions on*, vol. 27, pp. 370 –378, jan. 2012.

[20] H. Peyrl, G. Papafotiou, and M. Morari, "Model predictive torque control of a switched reluctance motor," in *Industrial Technology, 2009. ICIT 2009. IEEE International Conference on*, pp. 1 –6, feb. 2009.

[21] A. Bryson and Y. Ho, *Applied Optimal Control, Blaisdell Pub.* Co.: Waltham, Mass, 1969.

[22] S. Mattsson, H. Elmqvist, and M. Otter, "Physical system modeling with modelica," *Control Engineering Practice*, vol. 6, no. 4, pp. 501–510, 1998.

[23] J. Åkesson, K.-E. Årzén, M. Gäfvert, T. Bergdahl, and H. Tummescheit, "Modeling and optimization with Optimica and JModelica.org—languages and tools for solving large-scale dynamic optimization problem," *Computers and Chemical Engineering*, vol. 34, pp. 1737–1749, Nov. 2010.

[24] H. Hayashi, K. Nakamura, A. Chiba, T. Fukao, K. Tungpimolrut, and D. Dorrell, "Efficiency improvements of switched reluctance motors with high-quality iron steel and enhanced conductor slot fill," *Energy Conversion, IEEE Transactions on*, vol. 24, pp. 819 –825, dec. 2009.

[25] Y. Hasegawa, K. Nakamura, and O. Ichinokura, "Experimental verification of performance of a switched reluctance motor made of permendur," in *Electrical Machines (ICEM), 2010 XIX International Conference on*, pp. 1 –4, sept. 2010.

[26] H. Akita, Y. Nakahara, N. Miyake, and T. Oikawa, "A new core," *Industry Applications Magazine, IEEE*, vol. 11, pp. 38 – 43, nov.-dec. 2005.

[27] J. Widmer and B. Mecrow, "Optimised segmental rotor switched reluctance machines with a greater number of rotor segments than stator slots," in *Electric Machines Drives Conference (IEMDC), 2011 IEEE International*, pp. 1183 –1188, may 2011.

[28] R. Inderka, C. Carstensen, and R. De Doncker, "Eddy currents in medium power switched reluctance machines," in *Power Electronics Specialists Conference, 2002. pesc 02. 2002 IEEE 33rd Annual*, vol. 2, pp. 979 – 984 vol.2, 2002.

[29] H. Hayashi, K. Nakamura, A. Chiba, T. Fukao, K. Tungpimolrut, and D. Dorrell, "Efficiency improvements of switched reluctance motors with high-quality iron steel and enhanced conductor slot fill," *Energy Conversion, IEEE Transactions on*, vol. 24, pp. 819 –825, dec. 2009.

[30] G. Bertotti, "General properties of power losses in soft ferromagnetic materials," *Magnetics, IEEE Transactions on*, vol. 24, pp. 621 –630, jan 1988.

[31] J. Boivie, "Iron loss model and measurements of the losses in a switched reluctance motor," in *Electrical Machines and Drives, 1993. Sixth International Conference on (Conf. Publ. No. 376)*, pp. 219 –222, sep 1993.

[32] V. Raulin, A. Radun, and I. Husain, "Modeling of losses in switched reluctance machines," *Industry Applications, IEEE Transactions on*, vol. 40, pp. 1560 – 1569, nov.-dec. 2004.

[33] "Coercivity." `http://en.wikipedia.org/wiki/Coercivity`. Accessed: 2012-07-18.

[34] F. Blaabjerg, J. Pedersen, S. Sigurjonsson, and A. Elkjaer, "An extended model of power losses in hard-switched igbt-inverters," in *Industry Applications Conference, 1996. Thirty-First IAS Annual Meeting, IAS '96., Conference Record of the 1996 IEEE*, vol. 3, pp. 1454 –1463 vol.3, oct 1996.

[35] H. Le-Huy and P. Brunelle, "A versatile nonlinear switched reluctance motor model in simulink using realistic and analytical magnetization characteristics," in *Industrial Electronics Society, 2005. IECON 2005. 31st Annual Conference of IEEE*, p. 6 pp., nov. 2005.

[36] B. Venkataraman, B. Godsey, W. Premerlani, E. Shulman, T. M, and R. Midence, "Fundamentals of a motor thermal model and its applications in motor protection," in *Protective Relay Engineers, 2005 58th Annual Conference for*, pp. 127 – 144, april 2005.